ORIGINAL ARTICLE

# Methodologies for assessing the structural integrity of historic masonry domes and vaults

*Metodologias para avaliação da integridade estrutural de cúpulas e abóbadas históricas em alvenaria*

Danielli Cristina Borelli Cintra[a] (ID)
Deane de Mesquita Roehl[a] (ID)
Emil de Souza Sánchez Filho[b] (ID)
Paulo B. Lourenço[c] (ID)
Nuno Mendes[c] (ID)

[a]Pontifícia Universidade Católica do Rio de Janeiro – PUC-Rio, Programa de Pós-graduação em Engenharia Civil, Rio de Janeiro, RJ, Brasil
[b]Universidade Federal Fluminense – UFF, Programa de Pós-graduação em Engenharia Civil, Niterói, RJ, Brasil
[c]Universidade do Minho, Departamento de Engenharia Civil, Guimarães, Portugal

**Abstract:** Modern non-destructive investigation techniques and computational tools for nonlinear analysis allow understanding the structural behavior and damage of existing buildings, aiming at the least possible extent of intervention. Careful and minimal intervention is essential to preserve the authenticity of the built cultural heritage. An investigation with a historical, experimental, and numerical approach was carried out in the Theatro Municipal do Rio de Janeiro, in Brazil, a building with an eclectic architecture from the beginning of the twentieth century. Its masonry domes and vault have paintings by renowned artists on their intrados and were strengthened in the 1970s. The adopted methodology was based on anamnesis, characterization and observation of the structure employing non-destructive tests, and on the assessment of its vulnerability by nonlinear analyses of calibrated numerical models. Several hypotheses of differential settlement under gravitational actions were investigated, seeking to reproduce the cracking pattern and to identify the causes of damage to the masonry domes and vault before the strengthening. The nonlinear analysis of the structure allowed to evaluate the causes of the observed damage, assess the level of safety, identify the most vulnerable parts, and characterize the collapse mechanisms, in addition to demonstrating the efficiency of the intervention measures adopted in the past.

**Keywords:** non-destructive testing, non-linear analysis, masonry dome and vault, differential settlement, Theatro Municipal do Rio de Janeiro.

**Resumo:** Técnicas modernas de investigação não destrutiva e ferramentas computacionais para análise não linear permitem compreender o comportamento estrutural e danos em edifícios existentes, visando a menor intervenção possível. A intervenção cuidadosa e mínima é essencial para preservar a autenticidade do patrimônio cultural construído. Uma investigação de abordagem histórica, experimental e numérica foi realizada no Theatro Municipal do Rio de Janeiro, no Brasil, edifício de arquitetura eclética do início do século XX. Suas cúpulas e abóbada em alvenaria possuem pinturas de renomados artistas no intradorso e foram reforçadas na década de 1970. A metodologia adotada baseou-se na anamnese, caracterização e observação da estrutura por meio de ensaios não destrutivos e na avaliação de sua vulnerabilidade por análises não lineares de modelos numéricos calibrados. Diversas hipóteses de recalque diferencial sob ações gravitacionais foram investigadas, buscando reproduzir o padrão de fissuração e identificar as causas dos danos nas alvenarias antes do reforço. A análise não linear da estrutura permitiu avaliar as causas dos danos observados, estimar o nível de segurança, identificar as partes mais vulneráveis e caracterizar os mecanismos de colapso, além de demonstrar a eficácia das medidas de intervenção adotadas no passado.

**Palavras-chave:** ensaio não destrutivo, análise não linear, cúpula e abóbada em alvenaria, recalque diferencial, Theatro Municipal do Rio de Janeiro.

# 1 INTRODUCTION

Shell masonry elements, such as vaults and domes represent a widespread structural typology in historic buildings due to their aesthetic grandeur, symbolism, lightness, acoustic efficiency, and structural performance, covering from small to large spans. The study of the behavior of these structures received much interest from remote times to the present, using the most advanced analysis tools available [1]–[3]. One of the main causes of damage to masonry domes and vaults is the differential settlements of the foundations [4], which often come from underground works in the surroundings [5]–[7]. Monitoring the performance of masonry domes and vaults can contribute to the safety of the building itself, with the conservation of historical and artistic heritage, since they often have works of art integrated on their intrados, can also minimize the costs associated with corrective maintenance, restrictions on the use of the property, and even interdiction time in case of unacceptable safety level or major works. Since historic monuments are tourist attractions, their use and conservation are not only social but also economic demands.

Architectural heritage structures present a series of challenges for diagnosis and conservation due to the scarcity of construction records, diversity and variability of materials, restrictions on access and sample extraction, which limit the application of modern technical standards and building codes [8], [9]. The study of these structures requires a multidisciplinary approach, using iterative and sequential methodologies similar to those of medicine: anamnesis, diagnosis, therapy and control, which correspond, respectively, to the search for significant historical information, determination of the causes of damage and deterioration, choice of corrective measures and control of the efficiency of interventions [10]. For the understanding of the structural behavior and the existing damage in a building, aiming at the least possible extent of intervention, it can count on modern investigation techniques and advanced computational tools of analysis [11].

This paper presents an application of different combined techniques of diagnosis and analysis to evaluate the structural performance of masonry shells in a remarkable example of the Brazilian historical heritage, Theatro Municipal do Rio de Janeiro (TMRJ). The domes and vault have paintings by renowned artists on their intrados and were strengthened in the 1970s. Based on documentary research, the main design and construction characteristics of the building are presented, especially those of its shells, with a description of the structural evolution. Then, an experimental program was developed in order to investigate the current condition of the structure through visual inspection and characterization of materials and damage by non-destructive tests carried out in situ. The following were applied: i) remote method, such as photogrammetry [12]–[16] and infrared thermography [17]–[21]; ii) acoustic method, such as ultrasound [22]–[26]; iii) electromagnetic method, such as Ground Penetrating Radar [27]–[33] and rebar detection [34], [35]; iv) dynamic method [36]–[39]; v) deterministic method, such as the double flat jack test [40]–[42]; vi) qualitative method, such as the Masonry Quality Index [43]–[45]; among other methods.

Subsequently, a numerical model of the front part of the building using the finite element method was elaborated and calibrated. The interaction between ground and structure is studied for different conditions of soil stiffness, in order to identify the causes of damage reported in the structure in the 1970s.

Non-linear static analyses considering gravitational loads are performed to evaluate the load capacity of the shells in the original (before 1970s) and the strengthened condition, allowing to discuss the adequacy of the adopted strengthening. The analyses results are compared with experimental data to justify the damage that occurred before the past strengthening and to evaluate the current safety conditions of the structure.

# 2 HISTORICAL RESEARCH

TMRJ is one of the most imposing and beautiful buildings in Rio de Janeiro, considered as the main theatre in Brazil and one of the most important in South America. The architecture of the building is pointed out as the greatest representation of the eclectic style in Rio de Janeiro [46] and was inspired by the Palace Garnier in Paris. In an effort by the former Mayor Pereira Passos to modernize the city, which was the country's capital in that period, the TMRJ was built between 1905 and 1909 (Figure 1a, b) and can be divided into three main parts (Figure 1c): the entrance (with the foyer), the concert hall, and the scenic box (with the stage). The theatre, along with other monumental buildings in the vicinity with similar construction systems and architectural style

such as the National Library, the National Museum of Fine Arts and the old Amortization Bank, have been listed as a national historical and artistic heritage [47], since 1973.
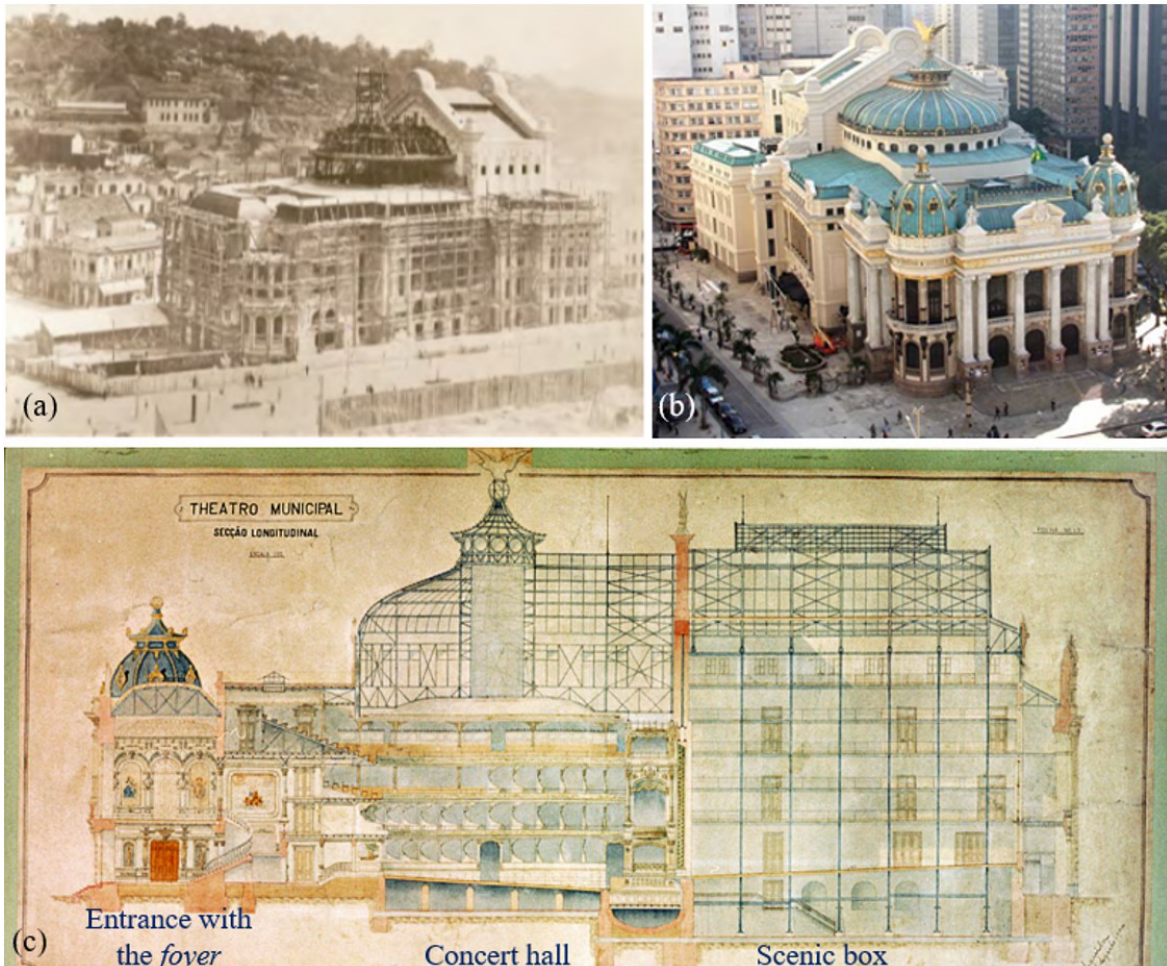


**Figure 1** – TMRJ: (a) roof building image by Augusto Malta (1906); (b) current facade; (c) longitudinal section by Francisco Oliveira Passos, 1904 [48]. *Source*s: (a; b; c) collection of Centro de Documentação do TMRJ (CEDOC).

## 2.1. Construction and structural characteristics

The TMRJ was built on a land of swampy soil, and about 1180 wooden friction piles with 4 m to 11 m length, were used for its foundation [49]. The structural system is made up of several materials (Figure 2a), including peripheral masonry walls, consisting of stones at the lower floor and solid clay bricks at the upper part, laid with mixed lime and cement mortar. As a fire prevention measure, the scenic box was protected by masonry walls of variable thickness, between 1.0 m and 1.8 m, with the opening of the stage protected by a metal curtain [48]. The 14 columns of the facade are made of a local gneiss and, internally, the floors are supported by massive columns and capitals of Italian and Belgian marble on the granite pedestals.

The concert hall was designed as a frame structure of steel elements, having as main parts 12 roof support columns and a large elliptical stucco dome, in addition to the cantilevers of the different levels of gallery. As these columns impaired the view of the stage, they were replaced by reinforced concrete trusses in 1934 [50]. The roof structure is composed of six trusses, linked together by braces and purlins [51].

In the main entrance of the TMRJ is the so-called noble area with the foyer (Figure 2b), a reception hall for the public, covered by a cylindrical barrel vault with intrados dimensions of 6.69 m x 17.42 m in plan view, with 2.60 m of rise, built in masonry with a double layer of clay bricks laid with mixed cement-lime mortar. The two side rotundas have a spherical dome roof, with a diameter of 6.28 m and with 2.75 m of rise, built of clay brick masonry laid with

mixed cement-lime mortar. These shells were built in 1907. They are supported on the entire perimeter by walls and columns. The domes will be addressed in relation to the neighbor street, namely as dome of Av. Treze de Maio and dome of Av. Rio Branco, left and right in Figure 2b, respectively.
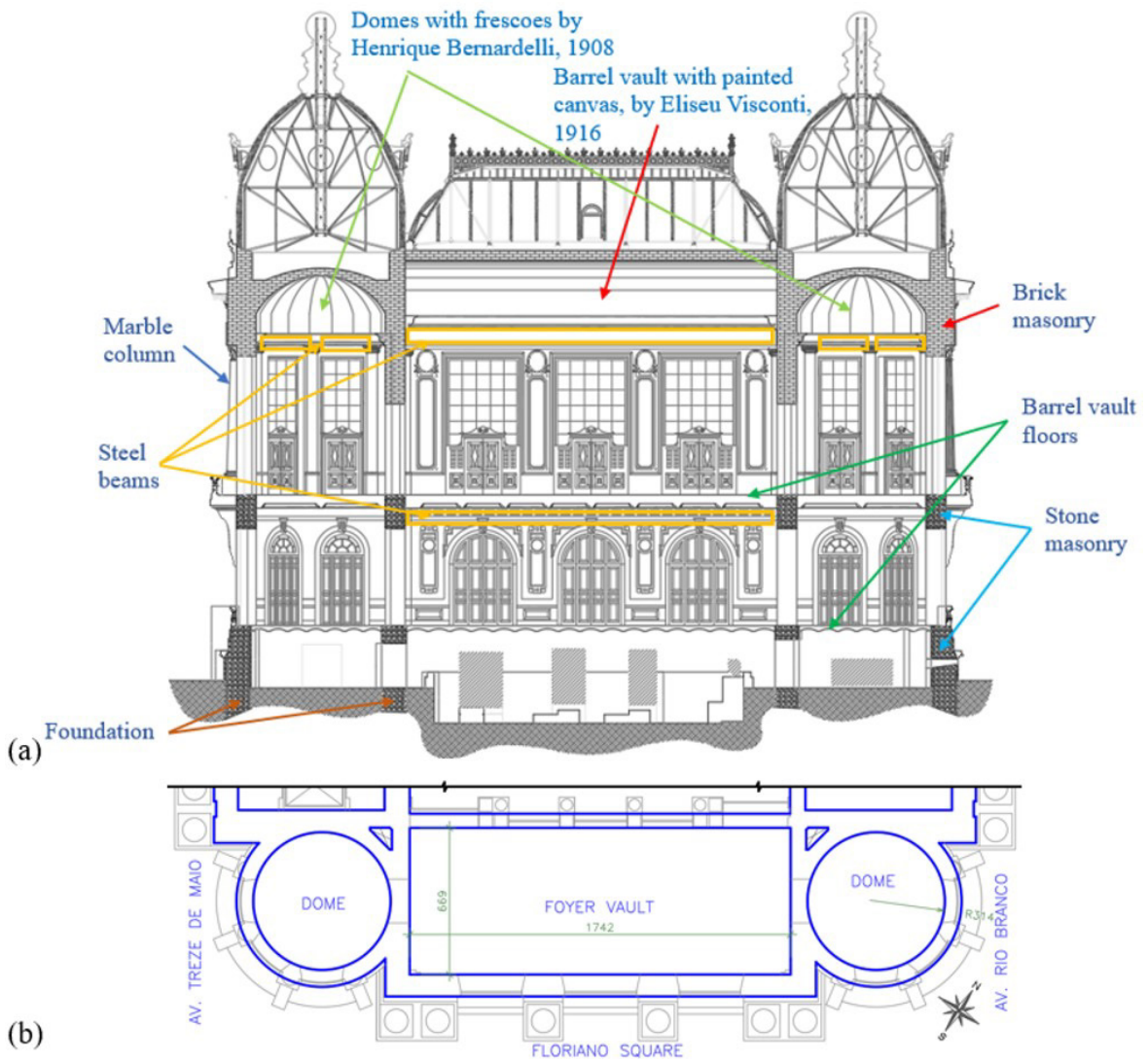


**Figure 2** – Details of the entrance: (a) cross-section; (b) plan of the noble area, including the domes and vault.

## 2.2. Works on the subway on Av. Treze de Maio

The first set of lines in the subway of Rio de Janeiro was inaugurated in 1979, after 9 years of construction, with Line 1 passing under Av. Treze de Maio, next to TMRJ (Figure 3a). In mid-1969, before the beginning of the works, an engineering consultancy hired by the subway company, carried out a geotechnical and foundation investigation of TMRJ. Inspection pits were executed at two points on Av. Treze de Maio, allowing access and direct inspection of the wooden piles (Figure 3b), which were in good condition, fully immersed in the water table, 1.9 m deep [12]. From then on, a permanent commission was formed to keep the structure of the TMRJ under constant observation.
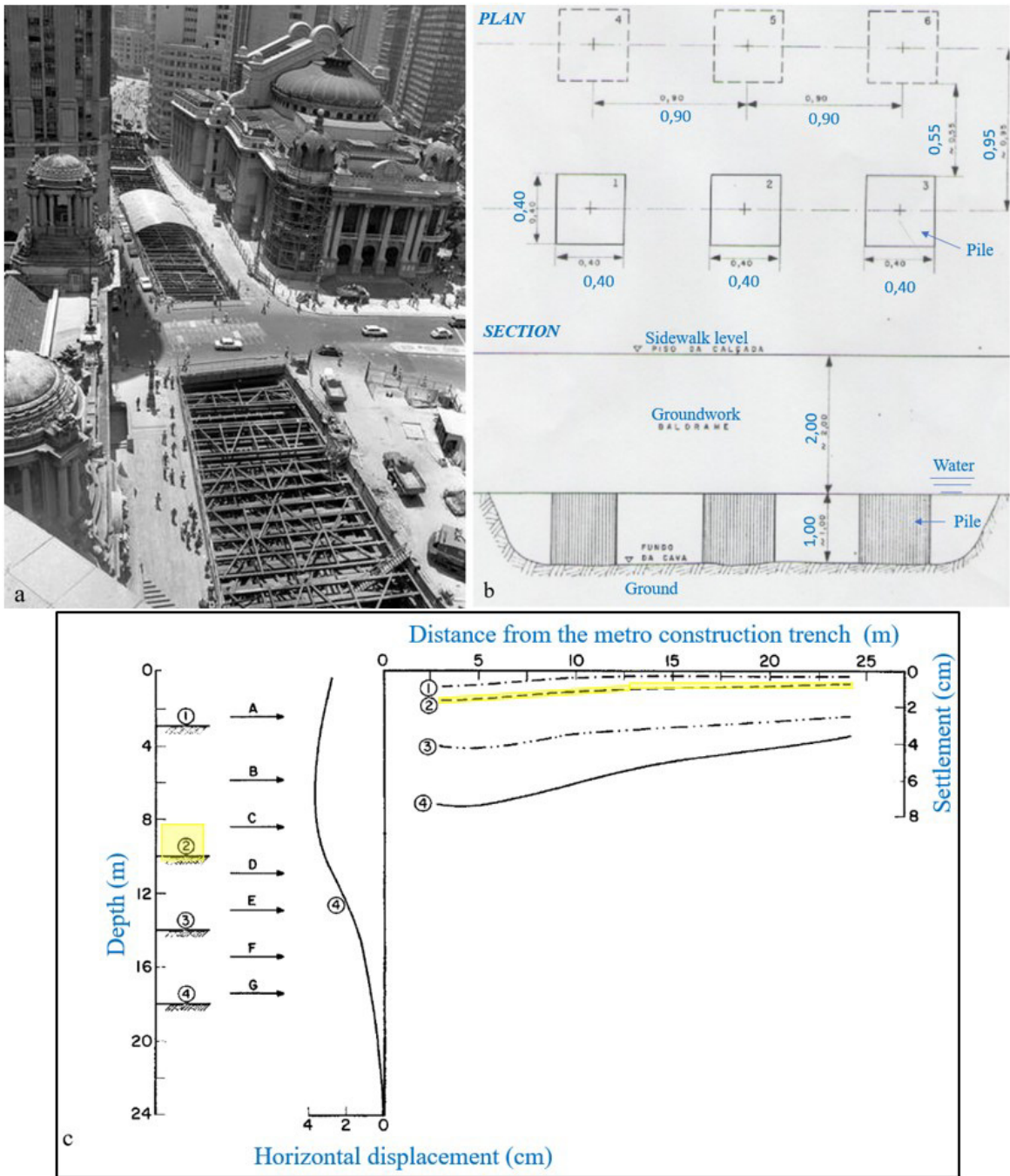
**Figure 3** – Construction of the subway in the 1970s: (a) overview of the trench next to TMRJ; (b) plan view and section of wooden piles in the foundations; (c) displacements measured in the subway construction trench at Largo da Carioca. Source: a) Photo – Paulo Moreira, 21/05/1975, https://acervo.oglobo.globo.com, access 07/12/2022 [52]; b, c) adapted from report [7], [53].

## 2.3. Strengthening of the masonry domes and vault

Lack of maintenance, festive events, vandalism, water infiltrations from the roof, construction works in the surroundings, such as the subway, among other events, damaged the building (Figure 4a, b). According to reports from the 1970's [54], [55], the paintings in the intrados of the masonry domes and vault were at risk of collapse mostly due to differential settlements and moisture in the masonry.
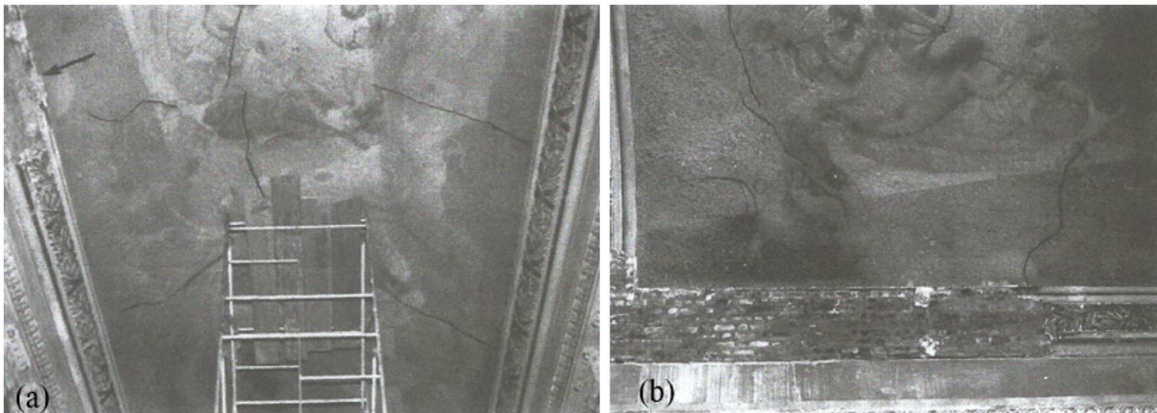
**Figure 4** – Photos of the damage in the vault in the 1970s, by Schiros [55]: (a) cracks; (b) moisture in the masonry.

In 1976, an intervention to strengthen the vault and the two domes was carried out in three days, without stepping on the shells and without shoring to avoid damaging the paintings on the intrados. The work consisted of the following steps [55]:

a) **step 1** – construction of reinforced concrete collar beams and an overlay of shotcrete reinforced with welded wire mesh at the extrados, as shown in Figure 5a. By casting, priority was given to the creation of arches crossing the largest transverse cracks (Figure 5b);

b) **step 2** – injection of epoxy resin in the cracks to restore the monolithism of the shells, using plastic tubes, according to Figure 5b;

c) **step 3** – fixing of metal anchors in drilled holes filled with epoxy resin, in order to promote adhesion between the original masonry shell and the new concrete overlay (Figure 5c, d).



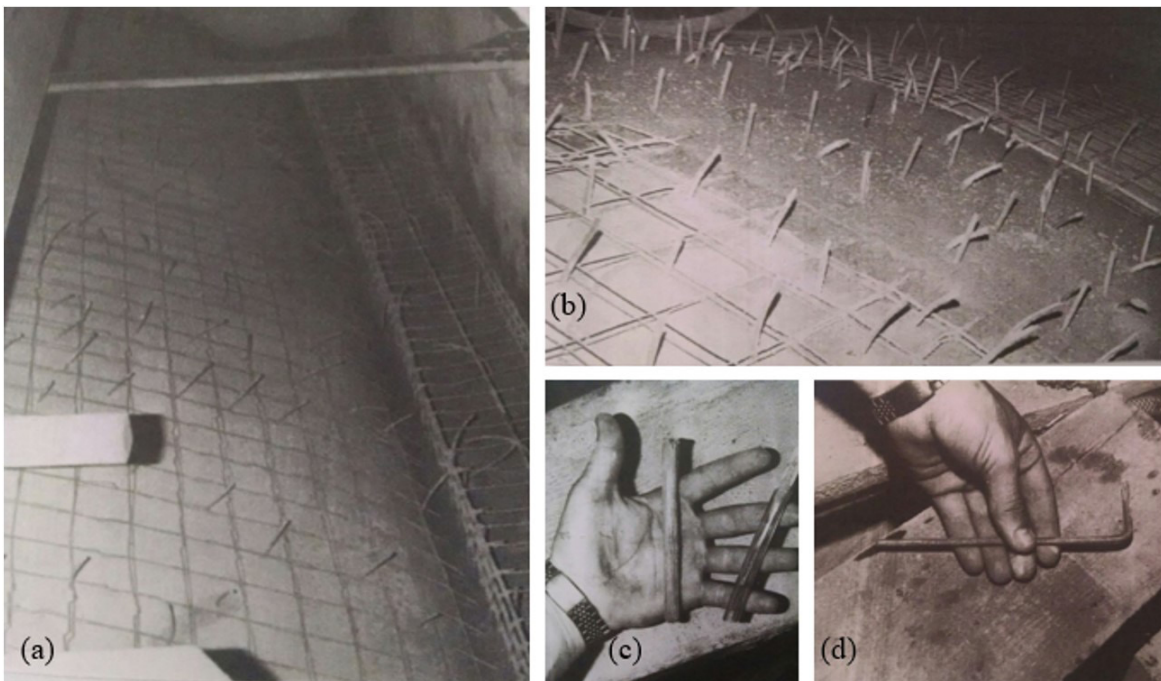**Figure 5** – Photos of the strengthening of the extrados of vault in the 1970s, by Schiros [55]: (a) reinforced concrete collar beam (right-side of the photo), with steel mesh in shotcrete layer and injection tubes for epoxy; (b) the creation of arches, using shotcrete; (c) resin injection plastic tubes for cracks filling and fixing of metal anchors; (d) detail of metal anchors for shotcrete overlay.

In 2012, three buildings, with 20, 4 and 10 floors, collapsed about 20 m from the back of the TMRJ, leaving more than 22 victims between dead and missing. This accident was attributed to inadequate structural interventions in one of the buildings, which also presented problems of differential settlement in the 1970s [56]. Finally, in April 2017 there was a small fire caused by an artefact thrown at one of the stained-glass window on the facade during a popular protest, but fortunately, the fire was promptly controlled. However, these events caused no serious damage to TMRJ.

## 2.4. Considerations about historical research

The documentary research provided the following information: (a) the building can be considered as a testimony of the technological advances in construction in the early 20th century, standing out the mixed structural solutions and the adoption of the most modern construction management tools of the time; (b) from the design stage, there was a concern to adopt measures that would increase fire safety, such as the specification of robust masonry walls to isolate the scenic box, while several buildings of the time suffered from successive fires and reconstructions; (c) similar effort to prescribe the most advanced techniques and materials for the time was also observed in the structural interventions that occurred after the construction, even if not necessarily correct in terms of modern conservation criteria; (d) the information collected in the revised documents was very useful for the interpretation of the tests presented next.

## 3 EXPERIMENTAL PROGRAM

The materials used in the building have unknown properties and are covered by the characteristic decoration of the eclectic style, making inspections difficult. To understand the internal constitution and integrity of the elements of the structure, an *in situ* non-destructive testing (NDT) campaign was developed, which the main results are presented below.

It is important to point out that the reliability of the mechanical properties obtained by non-destructive tests is considerably compromised without proper correlation with reference values obtained from semi-destructive or destructive tests. However, the combination of several techniques, care in the execution and knowledge of the factors that influence the results allow the interpretation of the data and validate estimates of the intended information [57]–[59].

## 3.1. Photogrammetry, infrared thermography, and damage mapping

The technique of short distance photogrammetry was applied in order to obtain the point cloud for digital and three-dimensional reproduction of the intrados of the domes and vault (Figure 6a). The point cloud generated has a density of 1 pixel per mm, a resolution of 9360 x 9360 pixels for the domes, and 44560 x 17000 pixels for the vault, with an accuracy of ±0.25 mm, which is satisfactory for the future detection of unevenness and discontinuities on surfaces. The comparison between point clouds obtained over time, from a reference spatial system, will allow detecting any rotation or lateral displacement of the supports, as well as vertical and horizontal movements of the shells, being a promising preventive monitoring tool due to its accuracy [4], specially indicated in case of interventions in the surroundings. The high definition of the orthophotos (Figure 6b-d) allowed the registration of works of art, particularly convenient for reference in future restorations of the paintings.

Passive infrared thermography with natural thermal excitation from insolation on the roof at the beginning of a summer afternoon, allowed to detect treated cracks (Figure 7a, b), the arrangement of the clay bricks (or masonry bond), hidden metal cramps (Figure 7b in blue), spots of moisture in the masonry (Figure 7c) and other construction details, all hidden by the works of art and decorative elements on the intrados and the concrete on the extrados. It is a useful tool for inspection and qualitative evaluation of masonry with a finished surface and difficult to access.
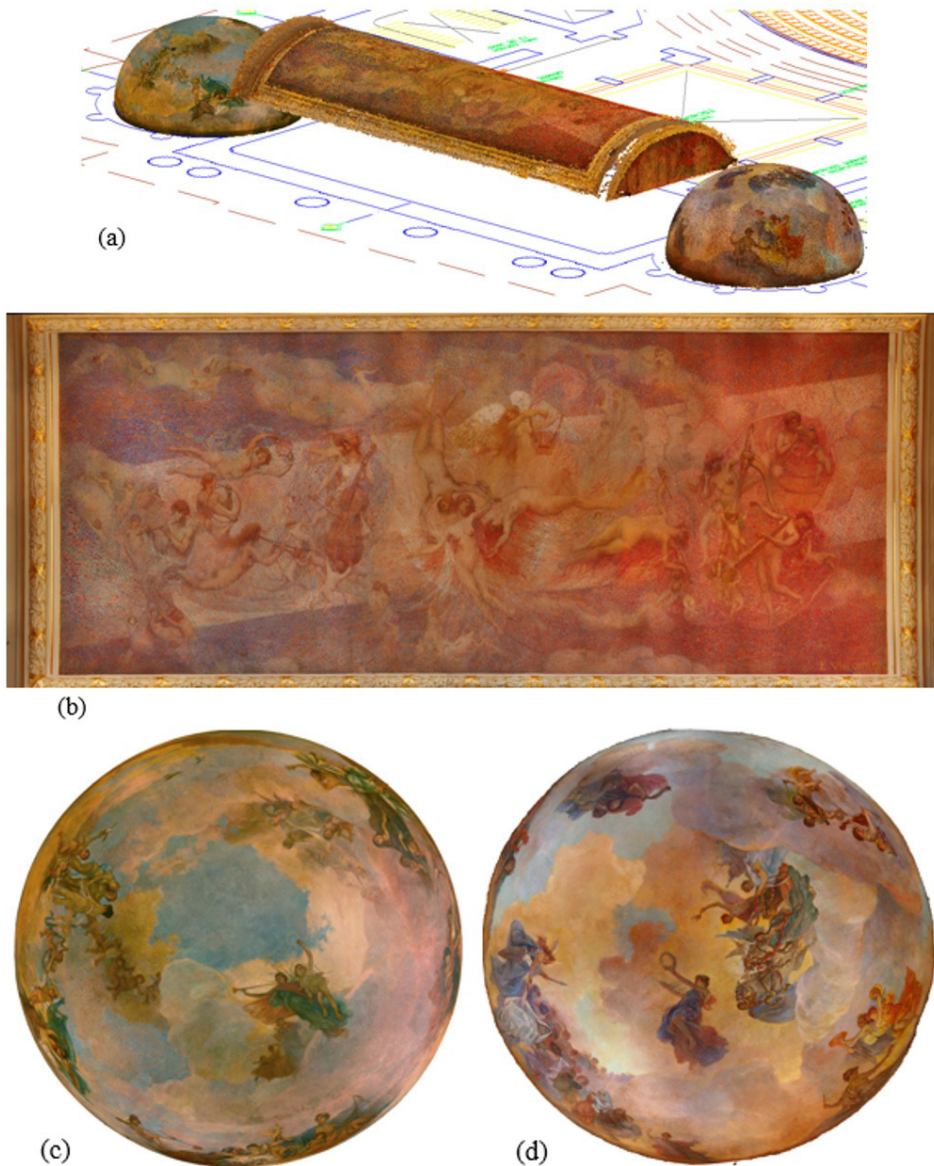
**Figure 6 –** Intrados of the domes and vault [60]: (a) point cloud; (b) orthophoto of the vault; (c) orthophoto of the dome of Av. Treze de Maio; (d) orthophoto of the dome of Av. Rio Branco. Images: Adolfo B. Ibáñez.
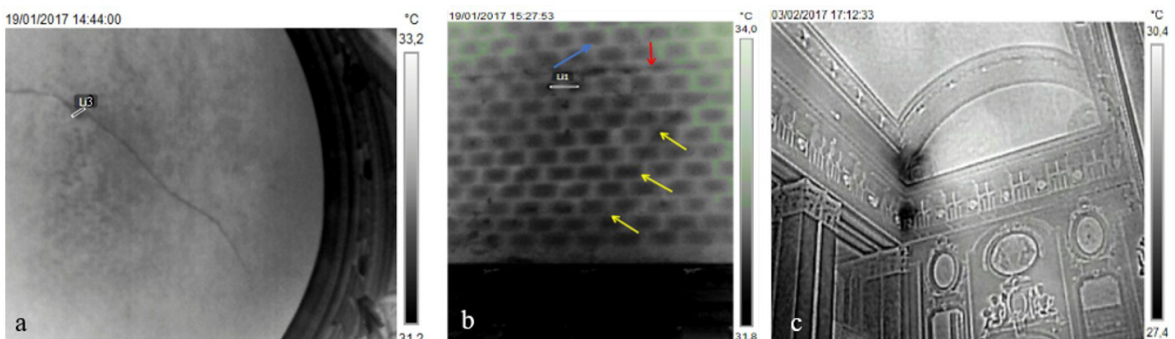


**Figure 7 –** Infrared image: (a) dome of Av. Rio Branco; (b) vault with indication of metal cramp in blue, treated cracks at the vertex in red and at the lateral in yellow; (c) moisture indication on the vault and walls. *Images: (a, b) Eduardo Azambuja; (c) Flávia Lamim.*

The images of photogrammetry and infrared thermography were used in a combined way to elaborate the damage map (Figure 8), which will be useful in damage monitoring, planning and control of future interventions, focusing on the trend towards interoperability with the use of advanced technologies such as Heritage Building Information Modelling (HBIM), Building Energy Modeling (BEM) and Artificial Neural Networks (ANN) [10], [61], [62]. Photogrammetry was applied to correct distortions in the thermal images from the curvature of the domes and vault.
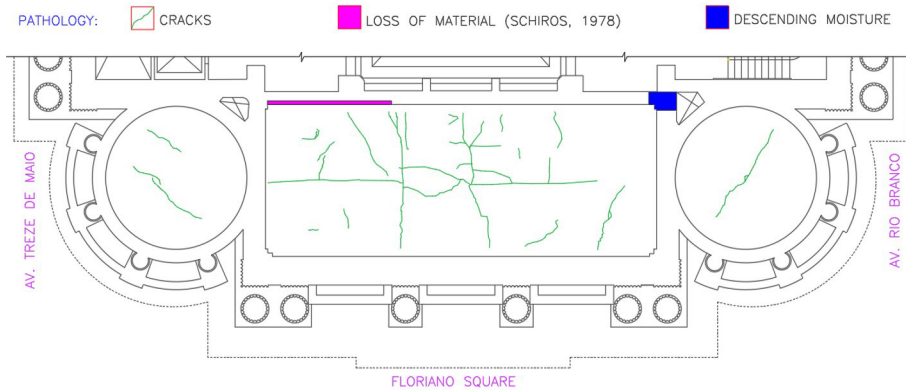


**Figure 8** – Damage map in the intrados of the domes and vault, with indications of the cracking pattern and loss of material that were treated in the 1970s, and the current moisture, all revealed by the thermography.

## 3.2. Rebar detection, rebound hammer, and ultrasonic propagation velocity tests

A rebar detector was used on the extrados (Figure 9) to map the steel rebars in the reinforced concrete applied in the 1970s, as well to identify original metal beams hidden by the decoration on the intrados. The cover of the rebars in the vault was estimated at 2.5 cm, which suggests a minimum thickness of the shotcrete layer of at least 3 cm, and the welded wire mesh has Ø3 mm wires, according to the time report [55]. Ø8 mm stirrups with an average spacing of 10.8 cm and a cover of 2.5 cm were detected in the longitudinal direction of the lateral collar beam. The rebar detector was also used to identify original metal beams hidden by the decoration, namely the beams of the jack-arch slabs with a span of 6.9 m and a spacing of 1 m, on the floor of the foyer, and the beams with a span of 4 m and a spacing of 0.8 m in the side corridors. This mapping helped in the execution of subsequent tests, allowing to deviate from the bars, minimizing their interference in the results.
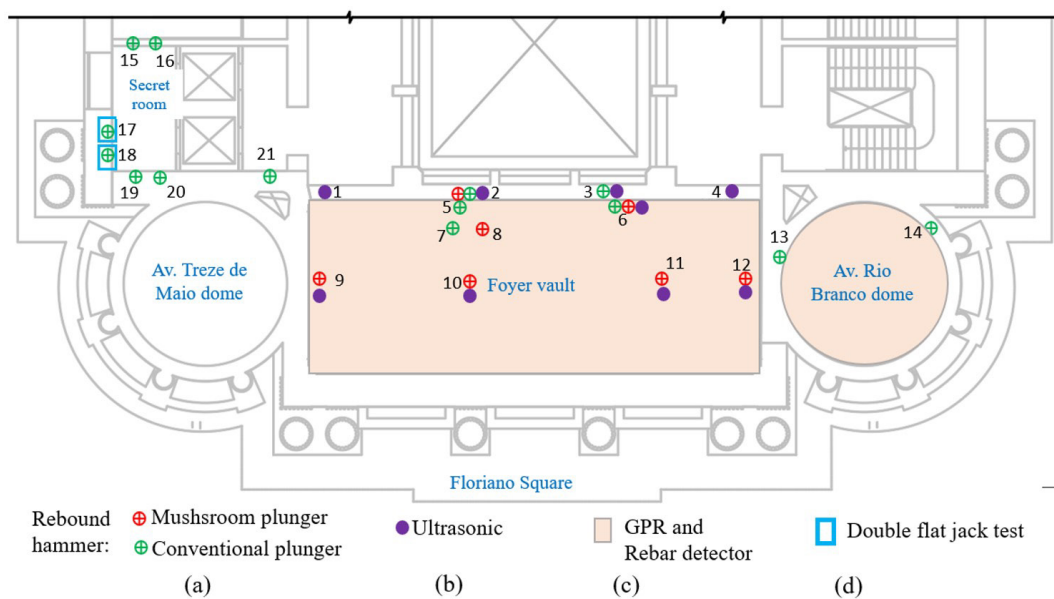


**Figure 9** – Plan with location of the tests.

The rebound hammer was useful for the qualitative assessment of the concrete used in the structure (Figure 9a), demonstrating little heterogeneity of the materials in each element studied [63]. Conventional and mushroom plungers were used, which is recommended by the equipment manufacturer for strengths between 5 and 30 MPa and elements with a thickness of up to 10 cm [64]. In each element of the structure, a similarity was observed between the results obtained with the same type of plunger, demonstrating the uniformity of quality and resistance of the materials that make up the same element. Measurements made with the mushroom plunger were on average 27% smaller than those obtained with the conventional plunger at nearby locations. Due to the infeasibility of removing cores from the structure, the results of this test could not be correlated with mechanical properties [60]. The ultrasonic wave velocity speed test with indirect transmission method was applied to evaluate the quality of the materials in the vault, concrete beam, and brick masonry walls to estimate their mechanical properties (Figure 9b) [65]. The distance of the transducers was controlled and the detection time of the P and R waves was measured from graphs of relative amplitude of the pulse as a function of the time it takes to travel from the transmitting transducer to the receiver [60]. The latter showed the lowest speed values (Figure 10), probably due to the greater porosity of the material and the presence of mortar joints. However, its results had a small variation, indicating little heterogeneity. As expected, the reinforced concrete beam had the highest wave velocity due to the presence of materials with higher density and low presence of voids. The vault showed intermediate velocities between the brick masonry and the concrete, indicating that the measurements probably incorporated the two types of materials that compose the domes and vault. The velocities were lower in the central region of the vault, possibly due to the presence of voids or cracks that, although treated, may have received the injection of mortar with a lower density than the masonry. Although most of the materials used in structures do not meet the conditions of the theory of elasticity, it is used to estimate mechanical properties, in the absence of more appropriate studies, requiring confirmation by other tests. Table 1 presents the dynamic modulus of elasticity ($E_d$) estimated from the velocity of longitudinal waves ($V_p$) and surface waves ($V_r$), Poisson's ratio ($v$) and the density of the material, using the theory of elasticity and assuming a homogeneous, isotropic, and elastic material (Equation 1). In the literature, there are variations of up to ±20% between the dynamic $E_d$ and static $E_c$ modulus of elasticity (Equation 2) [23], [25].
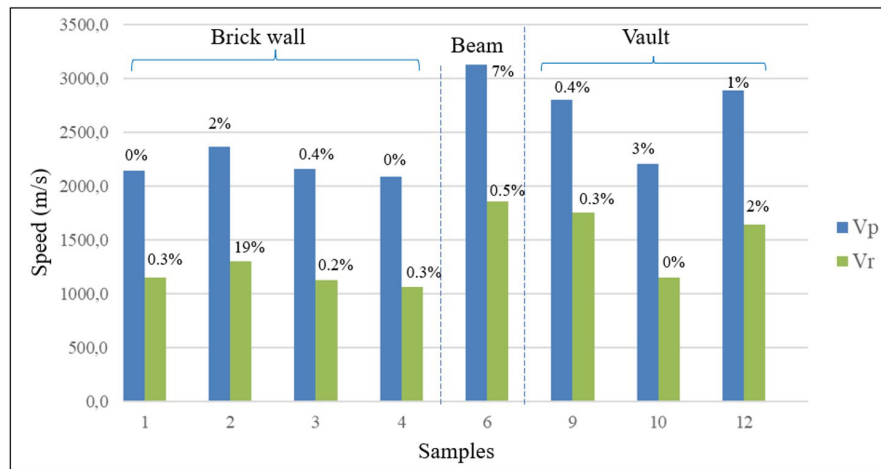


**Figure 10** - Average velocity of longitudinal ($V_p$) and surface ($V_r$) waves and standard deviation (%).

$$E_d = \frac{\rho V_p^2 (1+v)(1-2v)}{(1-v)} \tag{1}$$

$$E_c = \pm 20\% \, E_d \; [23], [25] \tag{2}$$

**Table 1** - Dynamic modulus of elasticity based on ultrasonic velocity tests.

| Element | $\rho$ (kg/m³) | $V_p$ (m/s) | $V_p/V_r$ (-) | $v$ (-) | $E_d$ (MPa) | $E_c = \pm 20\% E_d$ (MPa) |
|---|---|---|---|---|---|---|
| Brick wall | 1800 | 2191 | 1.89 | 0.27 | 6914 | 5531 to 8297 |
| Concrete beam | 2500 | 3131 | 1.68 | 0.20 | 19607 | 15685 to 23528 |
| Vault | 2000 | 2632 | 1.76 | 0.25 | 11084 | 8867 to 13300 |

## 3.3. Ground Penetrating Radar (GPR)

The GPR tests were carried out with 1.2 GHz frequency antennas and were useful to estimate the thickness of the domes and vault, the dimensions of the bricks, validate the construction characteristics, and detect hidden materials in the structure (Figure 9c) [60], [66]. 3D surveys were also carried out in each of the studied elements, but the radargrams were not considered satisfactory for analysis due to the high reflection of the steel net and consequent signal attenuation in the entire area below the net. Only in the sections where the bars were transverse to the path of the antennas, the signal was propagated along the section, allowing estimation of the desired information.

Figure 11a presents the construction characteristics of the dome of Av. Rio Branco and Figure 11b presents a typical radargram, in which a total thickness of the dome between 22 and 25 cm at the key is detected. The thickness grows towards the base, which appears to be 2 to 5 cm larger. In several radargrams, a pattern of small consecutive parabolas with spacing between 8 and 10 cm was observed in the alignment of the intrados, indicating the joint between bricks, whose dimensions are compatible with those found in the infrared images and in visible bricks in the adjacent wall. The steel bars of the wire mesh have a spacing of 10 cm, which is confirmed by the rebar detector and the description in old report [55]. No intermediate layer of masonry was identified, which confirms only one layer of brick in the domes.
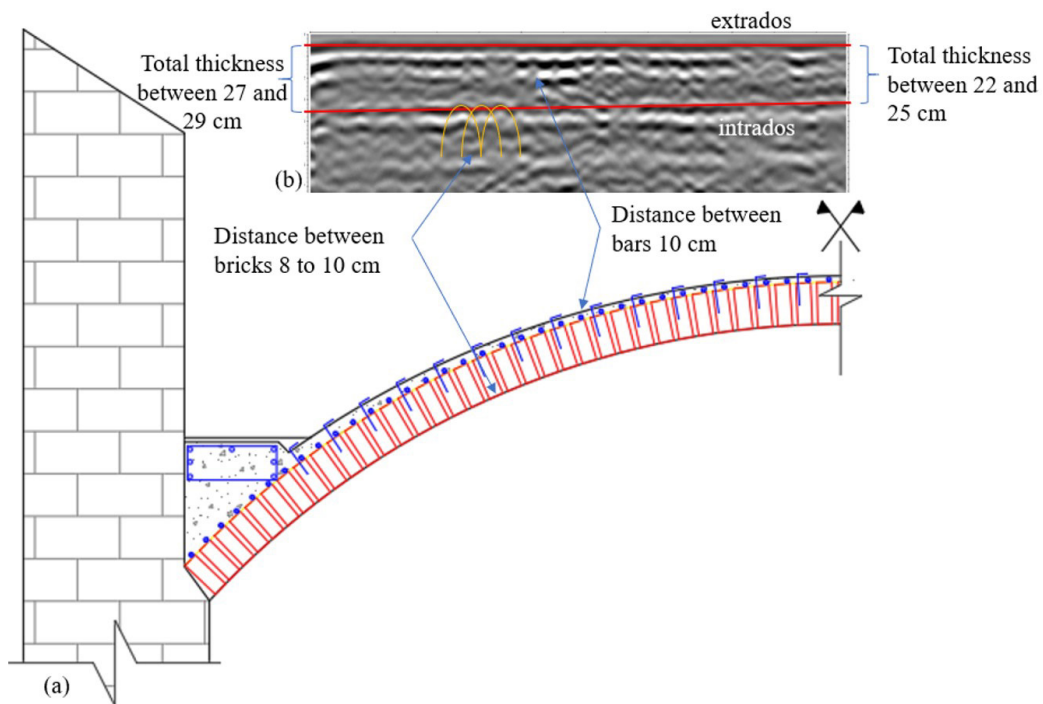


Figure 11 – Cross-section of Av. Rio Branco dome: (a) construction detail; (b) radargram [66].

## 3.4. Double flat jack test

Two monotonic double flat jack tests were carried out in brick masonry walls (Test I and Test II) to estimate the modulus of elasticity of the material, assuming that the tested walls are representative of the structure of the TMRJ (Figure 9d) [60]. After equipment calibration in the laboratory (Figure 12a) [67], a stress vs. strain diagram was obtained from the measurement of the displacements resulting from the application of axial load (Figure 12b) [68].

After some initial disturbance due to the accommodation of the flat jacks on the wall, the behavior of the masonry under increasing load was quite linear. A relevant increase of the horizontal dial indicator of Test I (Figure 12c, light blue line) was observed at a stress of 3.0 MPa, indicating the onset of cracking. Visible cracks appeared under stresses of 4.8 MPa, which corresponds to the second jump of the response on the horizontal dial indicator. The test was interrupted due to the limitation of the pressure capacity of the equipment at 6.0 MPa. The modulus of elasticity of the masonry was estimated at 5600 MPa by the slope of the trend line, with a value of $R^2$ of 0.998. The stress vs. specific strain diagram of Test II (Figure 12d), which was interrupted early due to equipment failure, indicates a modulus of elasticity in the same range, about 6500 MPa, with a value of $R^2$ of 0.990.

No reference value was found for the mechanical properties of this type of masonry in Rio de Janeiro. The results obtained in the double flat jack test can be considered close to the values found in the literature [41]. The average modulus of elasticity of brick masonry obtained by the flat jack test (6000 MPa) and by ultrasound (6900 MPa ±1400 MPa) are of the same magnitude, which offers greater consistency to the results obtained by both techniques.
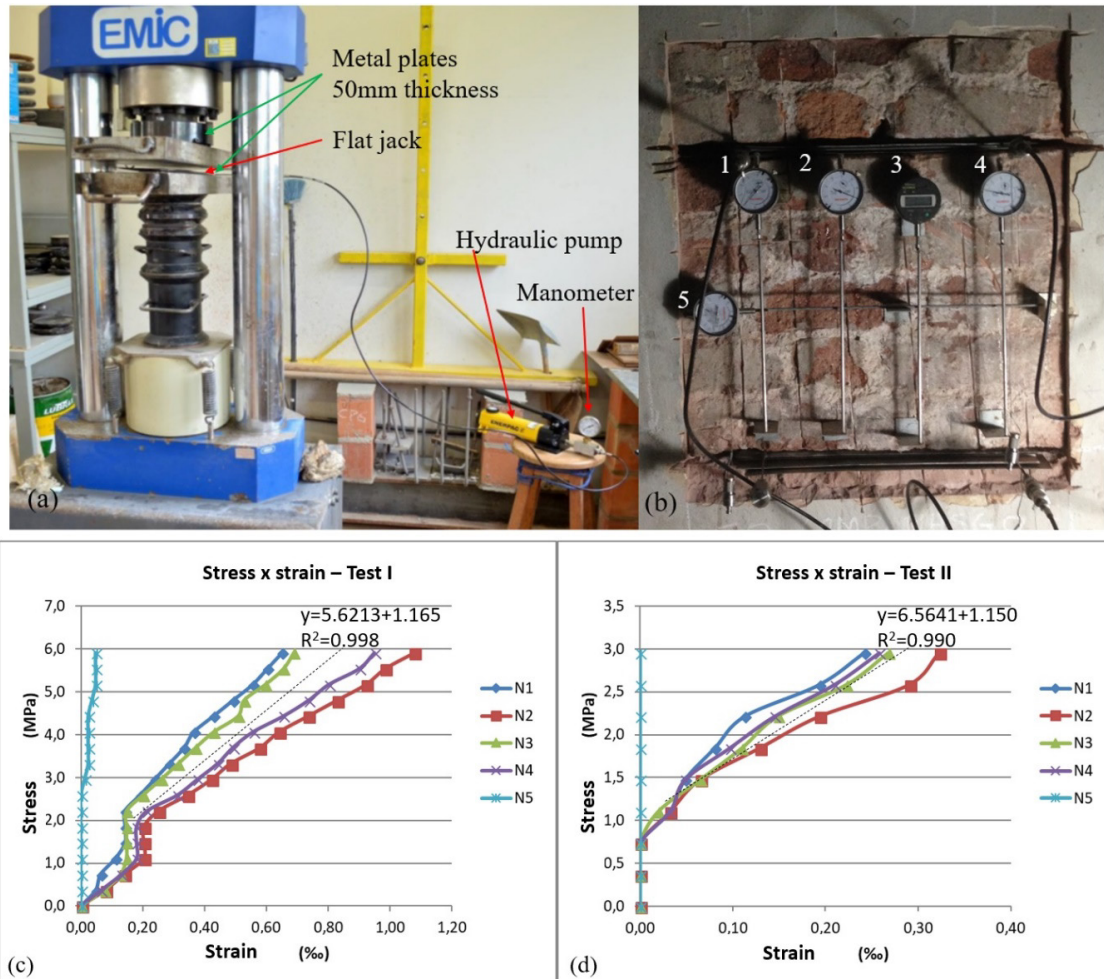


**Figure 12** – Double flat jack: (a) equipment calibration [67]; (b) test arrangement; stress x strain diagram to brick masonry (c) Test I; (d) Test II, interrupted early.

## 3.5. Masonry Quality Index (MQI)

Several authors resort to the recommendations of the Italian design code [69] to estimate the mechanical properties of masonry in the absence of experimental data for the analysis of historic structures [70], [71]. However, the Italian code does not contemplate the case of solid brick masonry with mixed cement-lime mortar. Therefore, the case of hollow brick with cementitious mortar was considered Table 2.

**Table 2 -** Values of masonry properties, according to the Italian code [69].

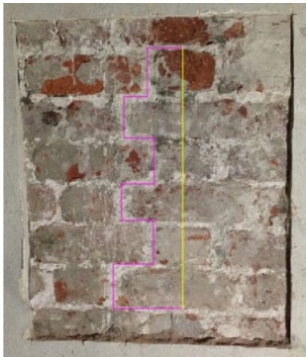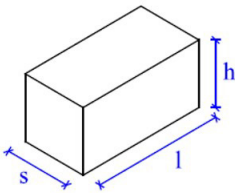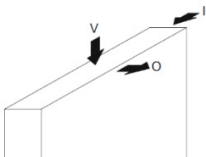| Masonry typology | Compressive strength $f_m$ (MPa) min-max | Shear strength $\tau_0$ (MPa) min-max | Elasticity modulus E (MPa) min-max | Shear modulus G (MPa) min-max | Specific weight (kN/m³) |
|---|---|---|---|---|---|
| Cut stone with good bonding | 2.6 – 3.8 | 0.056 – 0.074 | 1500 – 1980 | 500 – 600 | 21 |
| Hollow bricks with cementitious mortar | 5.0 – 8.0 | 0.24 – 0.32 | 3500 – 5600 | 875 – 1400 | 18 |

Another alternative is the MQI, whose objective is to visually evaluate selected construction parameters of performance of the masonry walls and correlate them to mechanical characteristics [43], [72]. By considering important factors necessary to assess the structural quality of a wall: mechanical characteristics and quality of the units (SM); dimensions of the units (SD); shape of the units (SS); level of connection between wall leaves (WC); horizontality of mortar bed joints (HJ); staggering of vertical mortar joints (VJ); quality of the mortar/interaction between units (MM)) this method allows to estimate several critical mechanical parameters of a masonry (compression strength ($f_m$); shear strength ($\tau_o$); Young modulus (E)) and is the most likely failure [45]. A numerical value is assigned according to the evaluation criteria of the method, and the MQI is calculated by Equation 3.

$$MQI = SM\left(SD + SS + WC + HJ + VJ + MM\right) \tag{3}$$

Properties estimated by the two approaches are now compared to those obtained experimentally. The value of the MQI is correlated to the properties of the Italian code through logarithmic curves proposed by Borri et al. [43]. Although the method is calibrated for masonry in Italy [44], [69], for lack of closer references, the Table 3 presents the MQI value and the estimate of the mechanical properties of the masonry of the brick walls of TMRJ. Figure 13 shows the values of the elastic properties of the brick masonry obtained through different methods, also including the database from the mid-20th century [41]. The compressive strength indicated by the Italian code for masonry of hollow bricks with cementitious mortar is slightly higher than those found in the literature for European buildings of the same period (Figure 13a). The results of the MQI analysis are high and go beyond the tension capacity of the flat jack used.

The values of the modulus of elasticity determined by the double flat jack test are close to those obtained in the ultrasonic tests, whose lower limit corresponds to the maximum suggested by the Italian code (Figure 13c). The results of the qualitative methods were more conservative than those of the experimental ones.

**Table 3 –** MQI analysis of TMRJ wall brick masonry.



**Description**

Regular masonry wall of ceramic bricks laid with cement mortar and lime, with a thickness of about 1.1 m. The joint thickness is between 1cm and 1.5 cm.

Typical brick dimensions:

h: 7.5 cm
l: 23 cm
s:11 cm

**Analysis**

| HJ | WC | SS | VJ | SD | MM | SM | Category | Vertical force (V) | Horizontal force in the plane (I) | Horizontal force outside the plane (O) |
|----|----|----|----|----|----|----|----------|--------------------|-----------------------------------|----------------------------------------|
| F | PF | F | F | PF | F | F | | A | A | B |
| | | | | | | | $M_{l\ surface}$ | | 1.83 | |
| | | | | | | | MQI | 9.0 | 8.0 | 6.0 |
| | | | | | | | Mechanical properties (min-max) | $f_m$ (MPa) | $\tau_o$ (MPa) | E (MPa) |
| | | | | | | | | 7.0 – 10.1 | 0.133 – 0.182 | 2620 – 3574 |

**Notes**: The possible classification for each parameter is fulfilled (F), partially fulfilled (PF) or not fulfilled (NF); Masonry behaviour is classified as inappropriate (C), medium (B) and good (A).
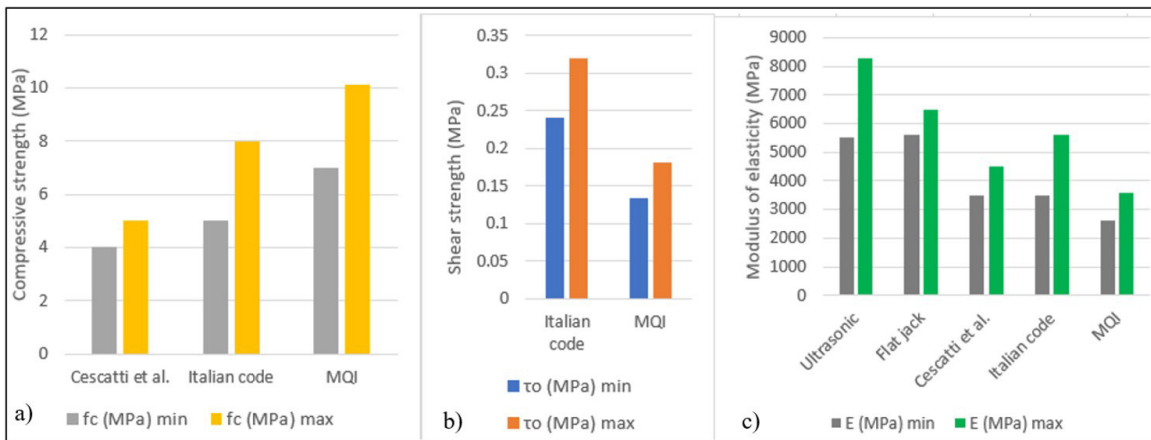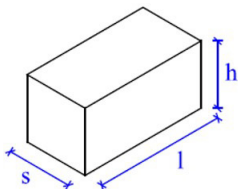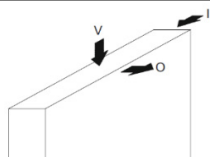
Rev. IBRACON Estrut. Mater., vol. 17, no. 4, e17406, 2024

13/29

**Figure 13** - Elastic properties of brick masonry by different methods ($f_c$ means compressive strength; $\tau_o$ means shear strength and E means elasticity modulus).

Table 4 presents the definition of the MQI and the estimate of the mechanical properties of the stone masonry of the walls. Figure 14 shows the minimum and maximum intervals for the values of elastic properties of stone masonry defined by the MQI method and by the Italian code for cut stones with good adhesion. The values are close, and the difference between the limits is between 0 and 16%.

In the absence of experimental data, Table C8 A.2.1 of the Italian code [69] is recommended, which presented the information closest to the experimental data of this research. Both the Italian code and the MQI, although practical methods and with potential to consider the most relevant aspects that influence the mechanical properties of masonry, require studies to validate their application to the types of masonry found in Brazil, especially those of the beginning of the 20th century.

**Table 4 –** MQI analysis of TMRJ wall stone masonry.

<table>
<tr><td rowspan="2"><b>Description</b></td><td colspan="8"></td></tr>
<tr><td colspan="8">Irregular masonry wall of stones laid with cement and lime mortar, with a thickness of about 1.25 m. The joint thickness is between 0.5 cm and 1.5 cm.<br><br>Typical stone dimensions:<br><br>h: 17 cm<br>l: 25 cm<br>s: 17 cm</td></tr>
</table>

| | HJ | WC | SS | VJ | SD | MM | SM | Category | Vertical force (V) | Horizontal force in the plane (I) | Horizontal force outside the plane (O) |
|---|---|---|---|---|---|---|---|---|---|---|---|
| | NF | PF | PF | PF | PF | F | F | | B | B | C |
| | | | | | | | | $M_{l\ surface}$ | | 1.57 | |
| | | | | | | | | MQI | 5.0 | 5.0 | 2.5 |
| | | | | | | | | Mechanical properties (min-max) | $f_m$ (MPa) | $\tau_o$ (MPa) | E (MPa) |
| | | | | | | | | | 2.9 – 4.6 | 0.056 – 0.082 | 1307 – 1859 |

**Note**: The possible classification for each parameter is fulfilled (F), partially fulfilled (PF) or not fulfilled (NF); Masonry behaviour is classified as inappropriate (C), medium (B) and good (A).
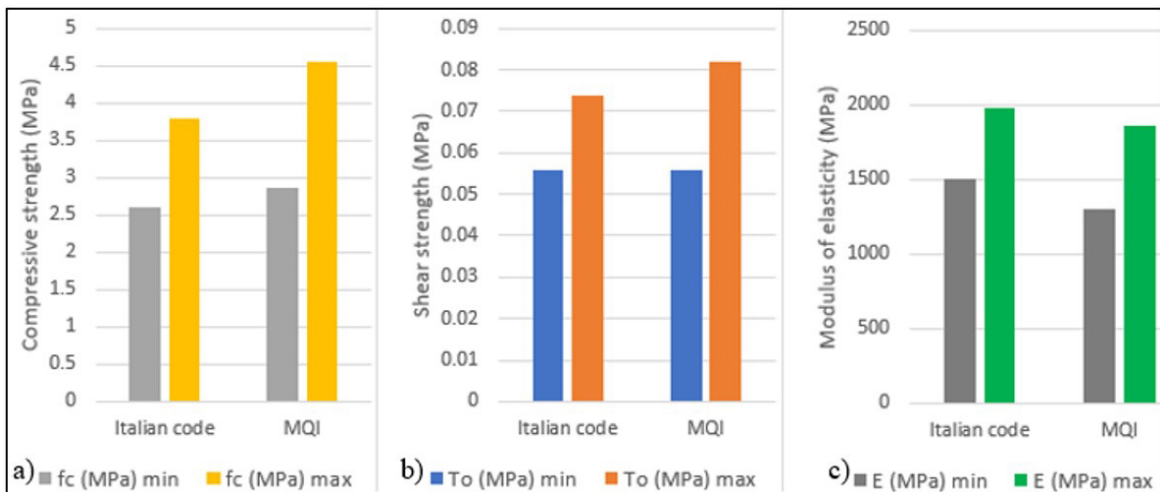
**Figure 14** - Elastic properties of stone masonry by qualitative methods ($f_c$ means compressive strength; To means shear strength and E means elasticity modulus).

As monitoring, it is possible to establish the points of the structure that are most susceptible to the weather and keep the windows with exposed masonry to visually assess or through image analysis the degradation of the mortar over time, which influences the parameter quality of the mortar/interaction between units (MM). It is common to observe in masonry with lime and clay mortars exposed to the weather. For architectural heritage, it will not always be possible to keep exposed masonry in strategic locations.

### 3.6. Dynamic identification tests

Dynamic identification tests were carried out to estimate the dynamic properties, such as natural frequencies and mode shapes, both at the global level of the building and at the local level of the domes and vault. The dynamic properties characterize the behavior of the structure with respect to the mechanical properties of the materials, construction system, existing damage, and boundary conditions. These were used to calibrate the numerical model (Section 4.3).

The acceleration of the structure caused by the ambient excitation, such as the action of the wind and the traffic of the subway and cars, were recorded using uniaxial piezoelectric accelerometers with the following characteristics: sampling frequency range of 0.15 to 1000 Hz, measuring range of ± 0.5 g, with 10 V/g sensitivity, coaxial cables, two acquisition boards with 24-bit resolution and a USB chassis connected to a laptop.

Independent measurements (setups) were carried out covering 14 different test configurations, in a total of 61 measured points, 12 of which were bidirectional. The series were correlated with each other using a fixed accelerometer as a reference for all setups. The tests were divided into global tests (7 setups - Figure 15a), tests in the vault (4 setups - Figure 15b), and tests in the dome (3 setups - Figure 15c). The acceleration time series were acquired with a rate of 200 Hz, lasting 30 minutes in each setup. The data acquisition software was developed by the University of Minho and the ARTeMIS software [73] was used to process the acquired signals. The analysis of the acceleration-time records was performed using the Frequency Domain Decomposition (FDD) method [73], [74].

In the global test, vibration modes with frequencies up to 20 Hz were estimated, as there were difficulties in extracting modes at higher frequencies due to the low levels of excitation associated with environmental measurements. In the local tests of the vault, the vibration modes were estimated with frequencies up to 30 Hz, and in the dome, due to its large stiffness, up to 100 Hz. The first frequencies and modes of global and local vibration of each shell were considered representative of the dynamic response of the structure (Figure 16) for the calibration step of the numerical model (Section 4.2) [70]. The main global mode (2.82 Hz) is associated with a transverse movement of the building, strongly influenced by the scenic box body. The seventh mode identified in the global test (7.79 Hz) indicates the vertical movement of the central part of the vault, being the main mode of vibration of this element, whose frequency is close to that of its corresponding mode in the local test of the vault (7.13 Hz). Due to the low frequencies considered, the global test did not identify any relevant movements in the domes, however, a mode with predominant vertical displacement of the vertex and with the base practically immovable was detected in the local test, with a frequency of 51.66 Hz.
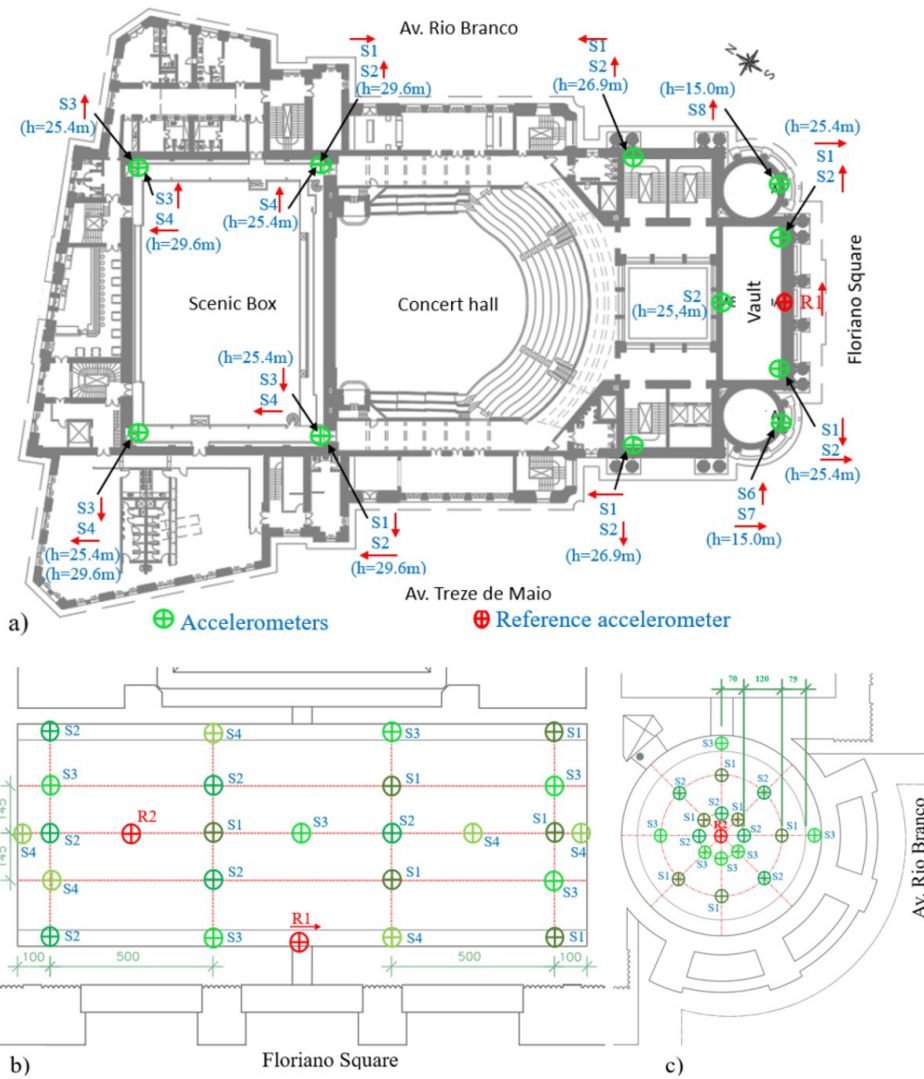
**Figure 15** – Configuration of the setups: (a) global; (b) vault; (c) dome (measurements in centimeters).

| Test | Main frequency (Hz) | Mode shape |
|---|---|---|
| Global | 2.82 |  |
| Vault | 7.13 |  |
| Dome | 51.66 |  |

**Figure 16** – Global and local modes.

## 3.7. Considerations about the experimental program

The experimental program was fundamental for the characterization of the structure (Table 5), providing data that: (a) confirmed and complemented the information from the documental research, such as geometric, constructive and mechanical properties data, which were verified by different tests; (b) it are useful for the elaboration and validation of the numerical model to be considered in the structural analyses presented next; (c) can be a reference for monitoring the integrity of the domes and vault and their incorporated works of art, allowing to control evolution of damage over time and during any future construction works in the surroundings; (d) can be a reference for the control of future interventions by advanced modelling technologies (i.e. HBIM, BEM and ANN), serving as a criterion for the assessment of changes in physical properties of the materials and proving guidance for selection of materials and techniques for conservation and rehabilitation actions. Although there are no signs of new cracks since the 1970s, it is recommended to ensure that the roof system is waterproof, as excessive moisture has been found in some walls.

**Table 5** – Experimental program carried out.

| Information obtained | | *In situ* tests | | | | | | | | |
|---|---|---|---|---|---|---|---|---|---|---|
| | | Photogrammetric | Thermography | Rebar detection | Rebound hammer | Ultrasonic | GPR | Double-flat jack | MQI | Dynamic identification tests |
| **Characterization** | Damage mapping | X | X | | | | | | | |
| | Moisture | | X | | | | | | | |
| | Mapping of non-visible elements | | X | X | | | X | | | |
| | Curvature and unevenness of shells | X | | | | | | | | |
| | Shell thickness | | | | | | X | | | |
| | Material homogeneity | | | | X | X | X | | X | |
| | Mechanical properties | | | | | X | | X | X | |
| | Numerical model calibration | | | | | | | | X | X |
| | Recording of works of art | X | | | | | | | | |
| **Monitoring** | | X | X | | | | | | X | X |
| **Control of interventions** | | | X | | | X | X | | | X |

## 4 NUMERICAL ANALYSIS

After the historical analysis and the development of the experimental program, the next step was to evaluate the structural performance of the domes and vault of the TMRJ before and after the strengthening carried out in the 1970s, focusing on the level of safety under gravitational loads, further extending preliminary studies carried out [75]. As shown in Figure 17, two models are considered for the entrance (with and without soil-structure interaction).

The adopted sequence of structural analysis using the finite element method in the DIANA software [76] is as follows: (a) a preliminary linear static analysis as model validation and to understand the behavior of the structure; (b) modal analysis to obtain the frequencies and mode shapes. These were calibrated with respect to the experimental results obtained from the dynamic identification tests; (c) non-linear static analysis under gravitational loading, considering the effect of soil-structure interaction and discussing the structural safety of the domes and vault.
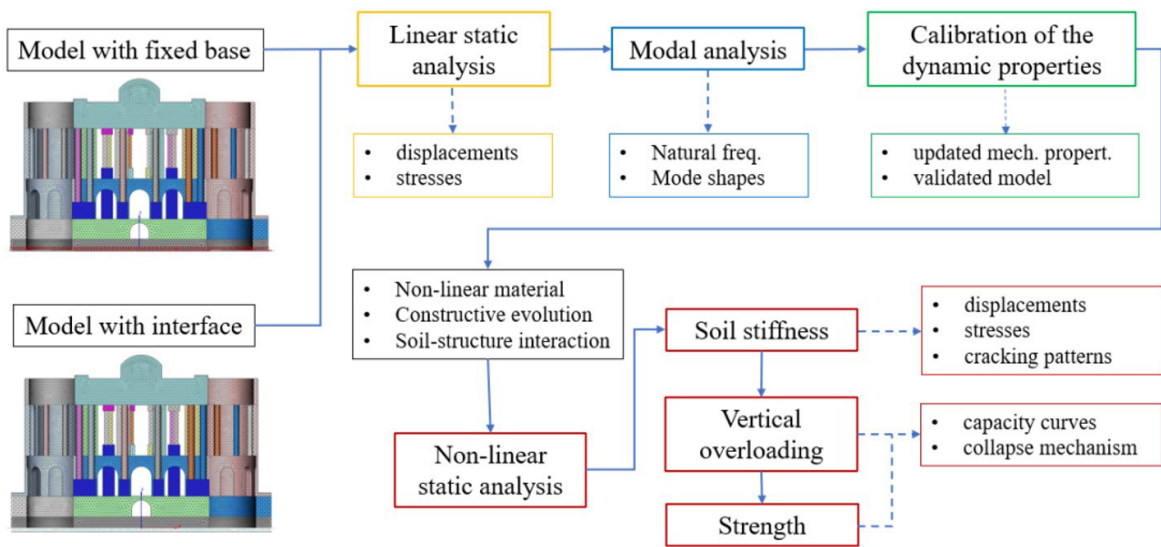
Rev. IBRACON Estrut. Mater., vol. 17, no. 4, e17406, 2024

17/29

**Figure 17** – Scheme of the numerical analysis performed.

The numerical model consists of 1,485,894 solid tetrahedral elements that represent the masonry, the stones, and the concrete, 8,742 triangular shell elements for the jack-arch slabs, 196 beam elements for the metal beams simply supported on the walls, 2,690 three-dimensional flat triangular elements to represent the interface between the foundation and the ground, and 1,410 one node translation spring elements to represent the axial stiffness of the walls omitted in the model. The adopted finite elements consider a linear interpolation of the displacement field with a total of 4,481,552 degrees of freedom.

For the initial phases of the structural analysis, all degrees of freedom of the nodes at the base level are restricted, providing a clamped boundary condition for the walls. Subsequently, in the soil-structure interaction analysis, the boundary conditions at the base were also evaluated using interface elements. Only gravitational loads were adopted, considering the self-weight of the structure and of the roof. The properties of the materials of the model (Figure 18) like elasticity modulus ($E$), Poisson's ratio ($\nu$), compressive strength ($f_c$), compressive fracture energy ($G_c$), tensile strength ($f_t$), tensile fracture energy ($G_f^I$) and specific weight ($\gamma$) are given in Table 6. The linear properties of masonry were adopted from experimental data and the MQI analysis, for the other materials were based on studies carried out on similar materials [23], [77]–[80].
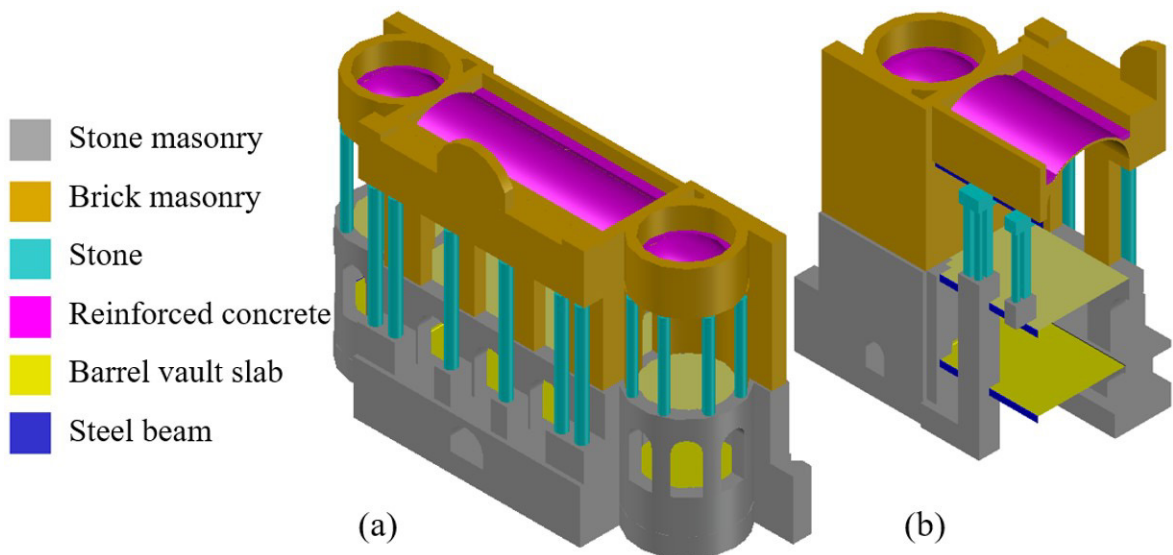


**Figure 18** – Identification of the different materials of the model: (a) front view; (b) sectioned back view.

Rev. IBRACON Estrut. Mater., vol. 17, no. 4, e17406, 2024

18/29

**Table 6** – Linear and non-linear properties of materials.

| Material | E (MPa) | Poisson (v) | $f_c$ (MPa) | $G_c$ (kN/m) | $f_t$ (MPa) | $G_f^I$ (kN/m) | $\gamma$ (kN/m³) |
|---|---|---|---|---|---|---|---|
| Stone masonry | 1350/1460* | 0.25 | 2.9 | 4.6 | 0.15 | 0.009 | 21 |
| Brick masonry | 6000/2632* | 0.25 | 6.0 | 9.6 | 0.30 | 0.009 | 18 |
| Stone | 5600/7025* | 0.25 | 11.0 | 17.6 | 0.50 | 0.030 | 25 |
| Reinforced concrete | 19000** | 0.20 | 16.0 | – | 4.50 | 0.126 | 25 |
| Barrel vault slab | 9000*** | 0.25 | – | – | – | – | 20 |
| Steel | 200000 | 0.3 | – | – | – | – | 78.5 |
| Sandy and compact soil | 70 | 0.3 | – | – | – | – | 19 |

*: values after model calibration; **: value based on similar material [78] to a reinforcement percentage of 0.5%; ***: proportion to the constituent materials.

## 4.1. LINEAR STATIC ANALYSIS

A linear static analysis was performed to check possible inconsistencies in the numerical model and to identify regions and elements associated with potential vulnerabilities, considering the gravitational loads and fixed supports in all directions at the base. A first validation was the comparison between the vertical reaction obtained through the analysis (47900 kN) and the one estimated by hand calculation (47800 kN), with a difference of 0.2%, attributed to the geometric approximation of the mesh.

A second validation was made from the displacements, which, in general, are small, considering only gravitational actions and fixed support conditions. According to the analysis (Figure 19a), the maximum vertical displacement of the structure is 5.6 mm and occurs in the central region of the vault, close to the internal support, which is composed of transition pillars, representing 0.08% or 1/1250 of its transverse span and 0.03% or 1/3121 of the longitudinal span. The range and distribution of displacements are in line with expectations and show that the most vulnerable part is likely to be the span between the entrance (foyer) and concert hall.

As a final validation, the stresses present in the linear behavior domain for all materials, with the maximum compressive stress being close to 0.7 MPa in the masonry, predicted for the granite columns and stone masonry of the facade (Figure 19b). The average compressive stress on the foundation is about 0.35 MPa, in accordance with the value foreseen in the hand calculation and in the report on the foundations [53].
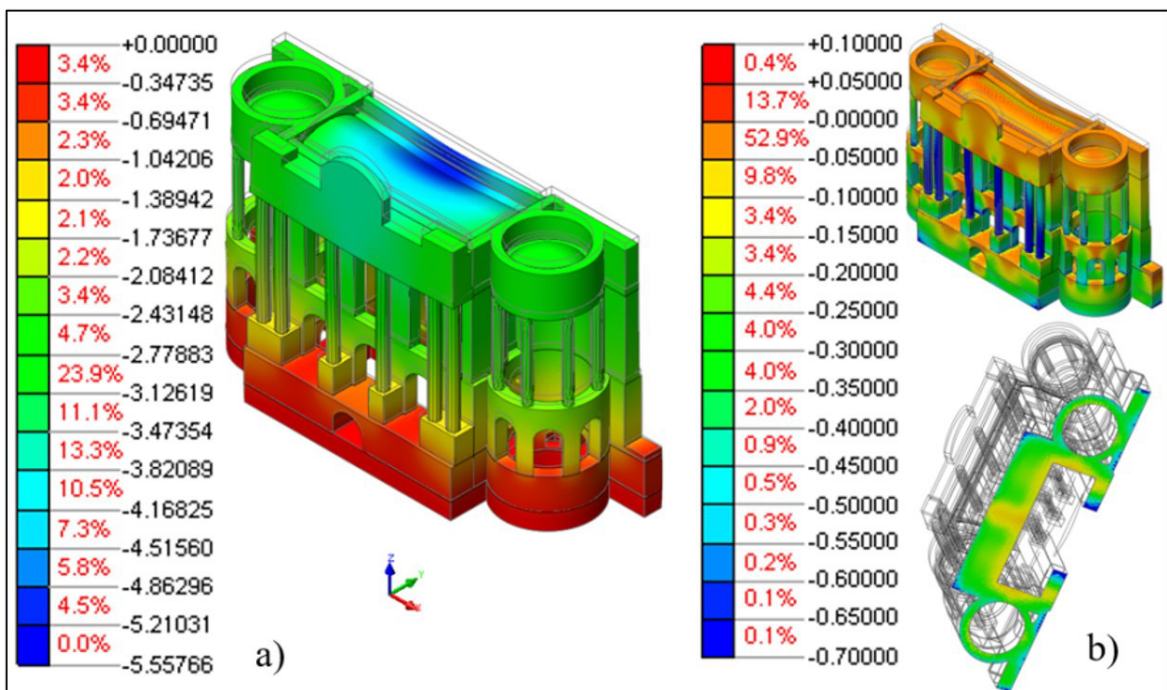


**Figure 19** – Linear static analysis: (a) vertical displacements (mm); (b) vertical stress (MPa).

Rev. IBRACON Estrut. Mater., vol. 17, no. 4, e17406, 2024

19/29

## 4.2. Eigenvalue analysis and calibration of the model

The eigenvalue analysis was carried out to validate the numerical model by comparing the results with the natural frequencies and mode shapes estimated through the dynamic identification tests (global modes and local modes of the dome and vault, which are presented in the Figure 20). Fixed support was considered in all directions at the base of the walls, assuming that from the conclusion of the subway works to the present day the soil conditions have been consolidated, without significant changes in the water table or settlements, it was considered that the boundary conditions are close to a rigid base. This also allows to update the model via a calibration process.
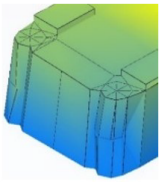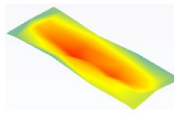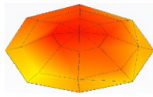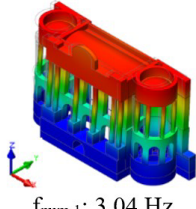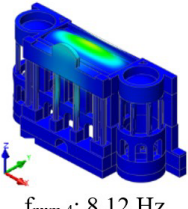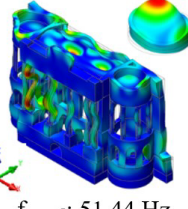
| Modal | Mode 1 (global) | Mode 2 (vault local) | Mode 3 (dome local) | Error (%) |
|---|---|---|---|---|
| Experimental | $f_{exp,1}$: 2.82 Hz | $f_{exp,4}$: 7.13 Hz | $f_{exp,5}$: 51.66 Hz | - |
| Numerical | $f_{num,1}$: 3.04 Hz | $f_{num,4}$: 8.12 Hz | $f_{num,5}$: 51.44 Hz | 7,8 |
| Calibration | 2,82 Hz | 7,13 Hz | 51,27 Hz | 0,25 |

Figure 20 – Comparison between the experimental and numerical modes before and after the calibration.

The first mode of global vibration (3.04 Hz) is associated with the lateral movement of the structure, strongly influenced by the stiffness of the stone masonry and by the mass of the elements of the upper part of the model. The first local mode of vibration in the vault (8.12 Hz) projects the element vertically, influenced especially by the stiffness of the marble columns and the brick masonry. The first local mode of the dome (51.44 Hz) corresponds to a vertical mobilization of the center of the dome, which appears as a very rigid element. The average error between the numerical and experimental results of the frequencies is 7.8% with the initial values adopted for the material properties, with an error of up to 5% being considered acceptable [81]. Judging that this error is due to the complexity of the construction, the simplifications adopted in the numerical model and the parameters involved in the calibration, it becomes necessary to calibrate the model properties of the most relevant materials. It is noted that the two first modal analysis frequencies were higher than those obtained experimentally, indicating that the model is too stiff.

The numerical model was calibrated by means of eigenvalue analysis having as reference the natural frequencies of the dynamic identification tests. Considering fixed supports at the foundation, the modulus of elasticity of the materials were adjusted, namely stone and brick masonry and the stone columns. Possibly, the properties of the masonry of the shells and walls are different from the values adopted due to the construction characteristics. The modulus of elasticity of brick masonry determined experimentally proved to be high to represent the elements with this material in the model. Maximum and minimum limits were adopted from the MQI analysis of the masonry and different modal analyses were carried out, obtaining a set of frequency values. An optimization algorithm following the method of Douglas and Reid [37], [38] was applied, resulting in a set of updated values of modulus of elasticity of 1460 MPa, 2632 MPa and 7025 MPa, for stone masonry, brick masonry and the stone columns, respectively, indicated in blue in Table 6, representing about 108%, 44% and 125% of the experimental program values.

The updated frequencies are close to the experimental results, with an average error of 0.25% (Figure 20). Thus, the agreement between the modal and experimental results is acceptable, and it is possible to consider that the numerical model is able to represent the main dynamic characteristics of the structure.

## 4.3. Considerations for non-linear analyses

In the non-linear analysis with DIANA, the standard Newton-Raphson iterative method was used combined with an energy convergence criterion with a tolerance of 0.001. The constitutive model adopted, called Total Strain Crack Model (TSCM), simulates the tensile and compressive behavior of material through the relationship between stress and strain in Figure 21. The Rotating Crack concept was considered, in which the relationship between stress and strain is evaluated in the principal directions of the strain tensor, which defines the direction of the crack opening [82].
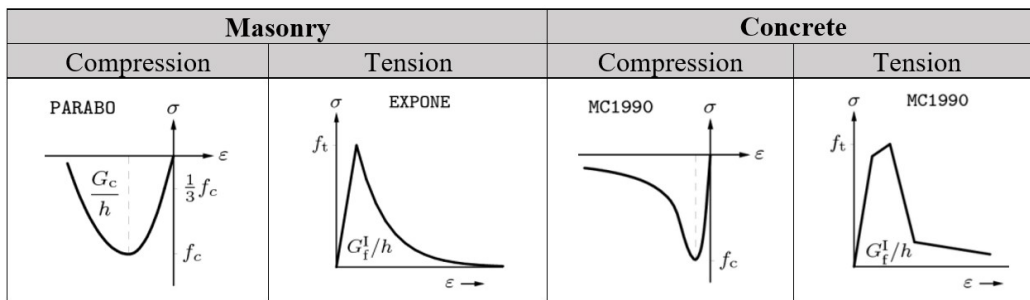


**Figure 21** - Non-linear behavior of materials [82].

The linear and non-linear parameters adopted for the materials are shown in Table 6. A phased analysis was performed simulating two stages of construction with rigid foundation. The first construction phase includes the building elements up to the top of the pillars, while the following phase includes the rest of the structure. The objective of this procedure is to better replicate the construction sequence and to cancel the displacements and damage due to the execution of the transition beam in the first phase, while maintaining a compression stresses state in the pillars. The case shown in Figure 22a provides the results of instantaneous load application in the entire structure. Then the elements of the first phase received the load of the other elements of the roof (case in Figure 22b), in a manner similar to what occurred in the construction process, considering the increasing stiffness of the structure with the progress of construction.
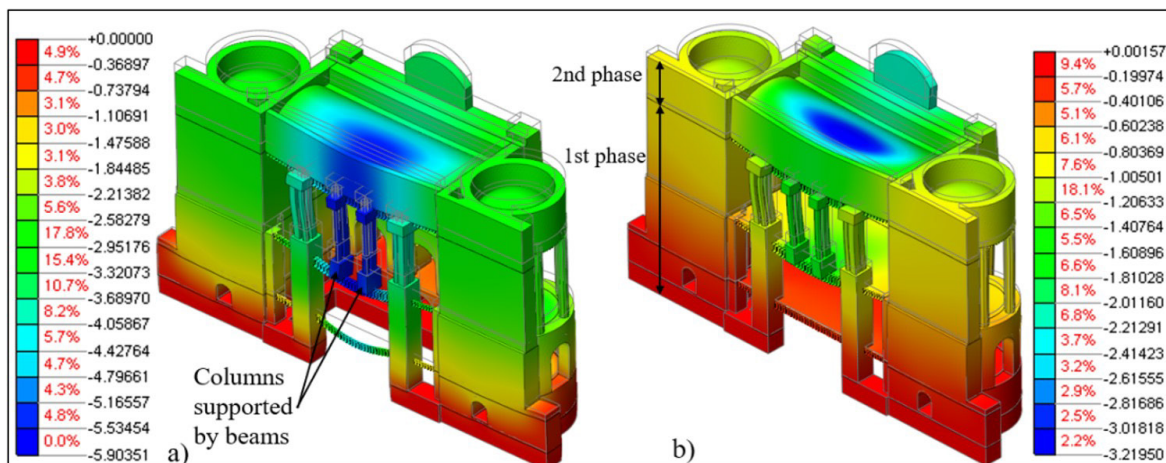


**Figure 22** – Vertical displacements (mm) of numerical model elements (%): (a) instant load; (b) with two construction phases.

As the gravitational actions were applied, the maximum displacement of the model remains very small, about 3.2 mm or 1/2200 of the span, occurring in the central part of the vault. This region is identified as the most vulnerable, although no significant crack was observed in the analyses. The displacement of the non-linear analysis in stages is smaller than the linear analysis (about 5 mm), which incorporated the displacements of the transition beam.

Soil-structure interaction was subsequently investigated. The hypothesis of an elastic interface for the foundation was adopted due to the uniformity of the piles and the short spacing between them, together with the fact that the walls are of

large proportions, which contributes to the uniform transfer of stresses to the soil (Figure 3b). It was considered that, until the 1970s, the soil stiffness conditions were constant along the entire foundation. A modulus of elasticity $E = 70$ MPa and the Poisson's ratio $\nu = 0.3$ for sandy and compact soil were assumed [80].

To validate the numerical model in the condition of flexible support, the coefficients of the vertical and horizontal reaction of the soil were estimated by the method proposed by Gazetas et al. [83] for foundations of different shapes, with geometric parameters represented in Figure 23. The values found are a vertical stiffness $k_v = 8920$ kN/m$^3$ and a horizontal stiffness $k_h = 4480$ kN/m$^3$, uniformly assigned to the interface elements with the soil. A non-linear analysis was again performed considering the gravitational loading. The average values of displacements found in the foundation (Figure 24) are close to the settlement estimated at $w = 28$ mm by the method proposed by Gazetas et al. [83]. Therefore, the stiffness of the soil attributed to the model was considered adequate to simulate the soil-structure interaction in the original condition of the construction.
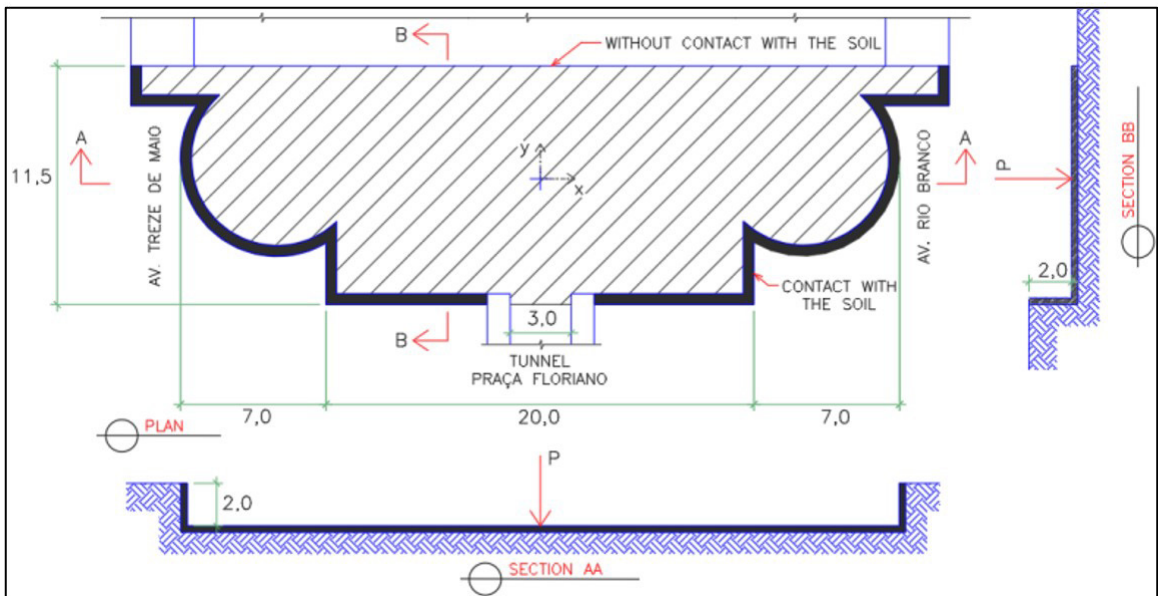


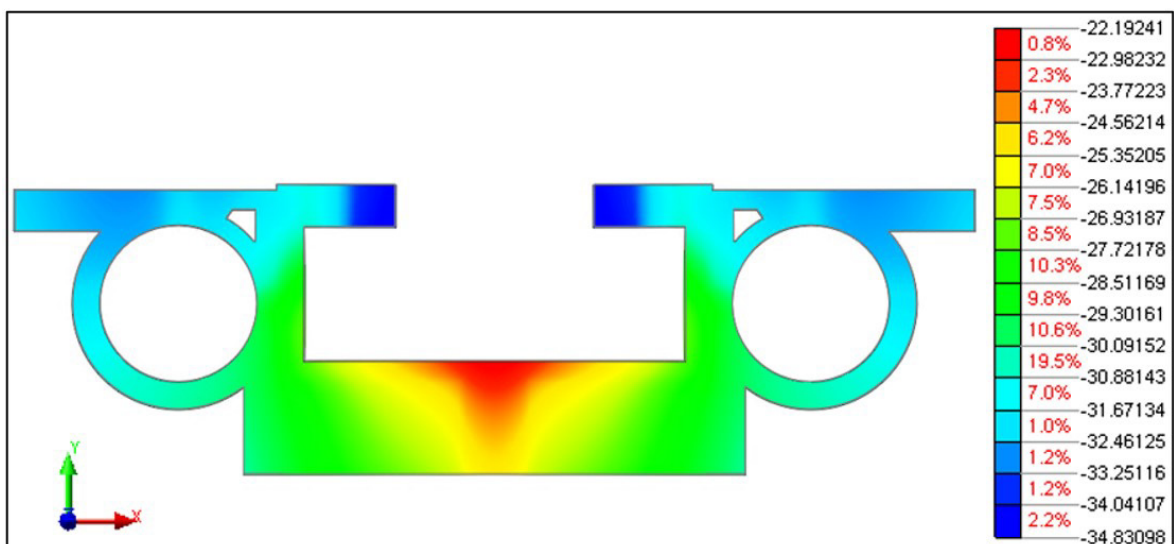**Figure 23** – Geometric parameters of the foundation, in meters.



**Figure 24** – Vertical displacements (mm) of the foundation in the last gravitational loading step.

According to the analysis, the difference in vertical displacements between the front and the rear parts of the structure reaches 12.6 mm or 1/560 of the span. This settlement is attributed solely to the process of deformation of the soil due to the weight of the building and occurred proportionally to the evolution of the construction, being minimized by the levelling of the floors. Therefore, it is considered that this initial settlement did not have a relevant effect on the shells.

## 4.4. Differential settlement analysis

Considering only the gravitational loads, non-linear analyses were carried out in three phases: the first and the second construction stages with fixed supports; a third stage with the completed construction with interface elements to study the soil-structure interaction. The damage obtained was compared to the pattern identified in the experimental program.

The Figure 25 shows the three scenarios, among several analyzed: (1) Case 1 - decrease of soil stiffness at the base of the main facade; (2) Case 2 - decrease of soil stiffness at the base of the walls and the pillar of Av. Treze de Maio; (3) Case 3 - decrease of soil stiffness at the base of both internal walls and the pillar of Av. Treze de Maio. The Case 3 presented a cracking pattern closest to the actual mapped damage (Figure 25), with a crack opening of 2 mm. This indicates that the differential settlement associated with a large soil settlement in the internal supports of the domes and the pillar of Av. Treze de Maio is likely to be the main cause of damage reported in the 1970s [54], [55].
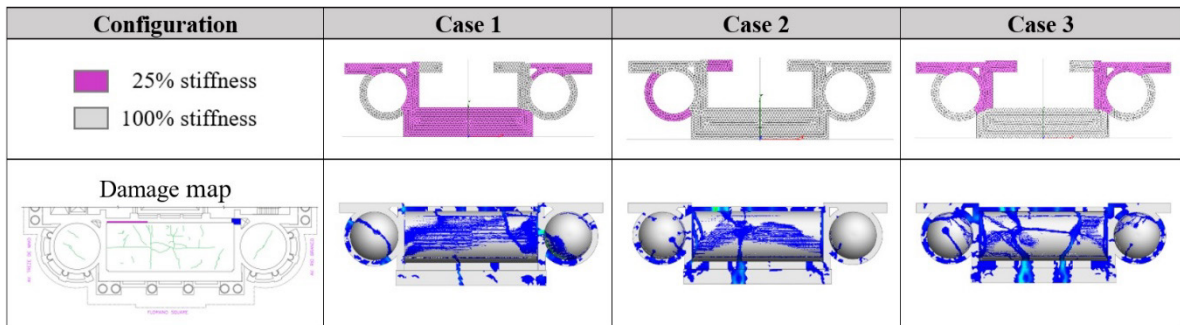


| Configuration | Case 1 | Case 2 | Case 3 |
|---|---|---|---|
| 25% stiffness / 100% stiffness | | | |
| Damage map | | | |

**Figure 25** – Configuration of cracks in the intrados of domes and vaul for the cases of non-uniform soil stiffness.

In Case 3, a reduction of 25%, 50% and 75% of the vertical and horizontal stiffness coefficient of the soil was analyzed. The points considered representative for the control and assessment of displacements in the structure are shown in Figure 26a. The vertical displacement at the base of the pillar of Av 13 de Maio with the gradual reduction of soil stiffness is shown in Figure 26b, which indicates the initial settlement of 32mm with the soil stiffness before the subway works. Considering that this base has characteristics similar to the foundations studied by Jucá [7], it is estimated that a settlement between 1 cm and 2 cm occurred during the excavations of the subway (Figure 3c), which corresponds to the effect of 75% to 50% of the soil stiffness, as highlighted in yellow in Figure 26b.
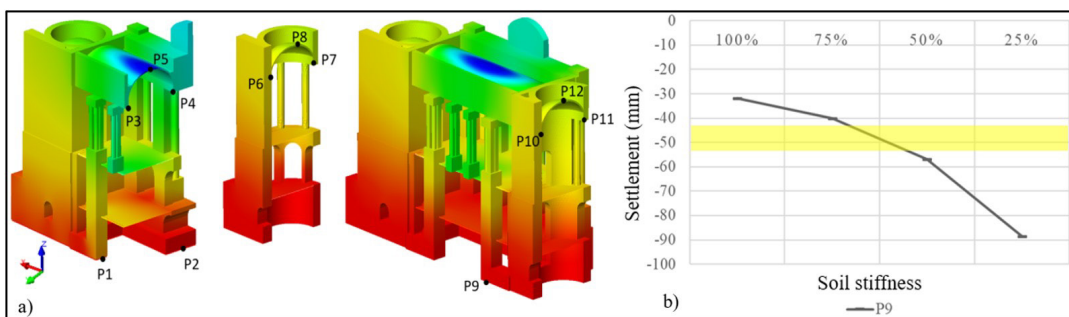


**Figure 26** – (a) Position of the displacement control points; (b) vertical displacement (mm) in P9 for Case 3.

The Figure 27 indicates the difference in displacements between the control points of the supports with the reduction of soil stiffness. The supports of the vault showed the highest rate of variation in vertical displacements (Figure 27a).

The supports of the dome of Av. Rio Branco had a greater difference in displacements than those of the dome of Av. Treze de Maio. This explains why the recorded damage [55] was more pronounced in the dome of Av. Rio Branco. In Figure 27b, the horizontal displacement is observed as a function of the reduction of the soil stiffness, with a marked variation in the supports of the vault, which leads to increasing action on the walls.
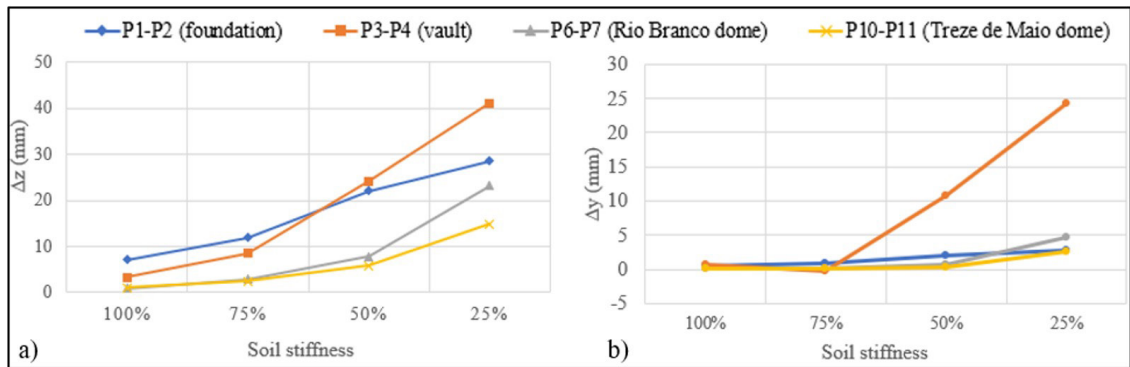


Figure 27 – Displacement (mm) for Case 3: (a) vertical; (b) horizontal.

## 4.5. Analysis of the gravitational load capacity

To evaluate the load capacity of the structure, the self-weight was progressively increased up to collapse, in the non-linear analyses performed considering the line search algorithm and the arc length method to stabilize the convergence of the iterative process and obtain the post-peak behavior [82]. The vertical load factor is defined by the relationship between the load applied and the structure's weight.

The Figure 28 shows the load capacity curve concerning the adopted control points in the domes and vault, considering two construction phases, without the reinforced. The vault (Figure 28a) maintains a predominantly linear behavior up to a load factor of 1.9. Then, cracks at the extrados of the supports appear, forming two hinges (Figure 29) and causing sudden drop in the response. The third hinge appears shortly afterwards, with the crack of the vault key in the intrados. However, the structure is still stable after this point, increasing the opening of the cracks, being able to withstand a vertical load about 3.7 times its weight. Then, collapse occurs due to the appearance of cracks in the support of the facade, forming the fourth hinge. The support of the facade showed greater displacements than the internal support since the latter is braced by the internal part of the building. The maximum vertical displacement occurs in the center of the vault, with 29 mm, corresponding to 1/240 of the span.

The domes proved to be much stiffer than the vault, reaching a load factor of 8.6 times its weight, still with linear behavior (Figure 28b). This factor corresponds to the load capacity limit of the model due to major damage in the brick masonry of the facade. The increase in the span of the domes was still insignificant at this very large load level.
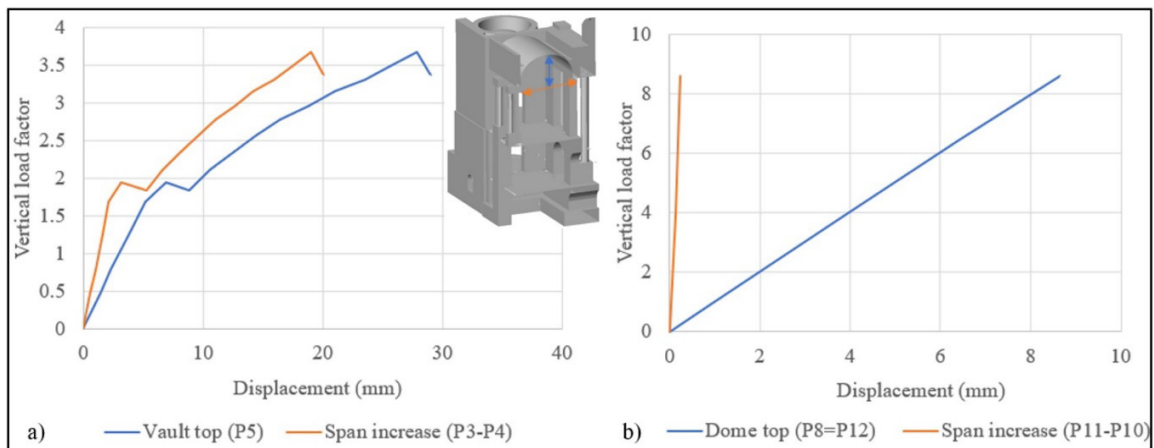


Figure 28 – Gravitational load capacity curve in the original building (before strengthening): (a) vault; (b) dome.
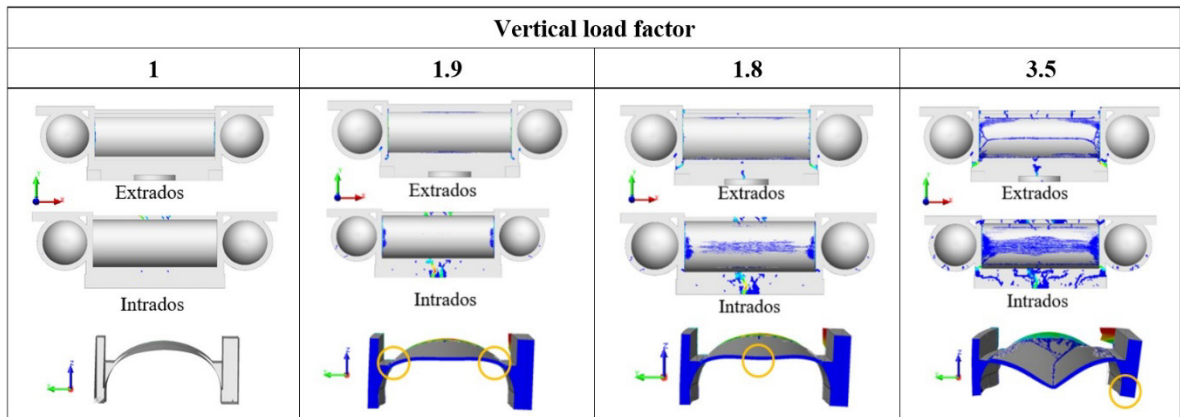
**Figure 29** – Collapse mechanism due to gravitational loads in the original model.

The efficiency of the strengthening in the vault is evaluated by a comparison between the load factors in the original and strengthened condition, concerning the vertical displacements at the vault key (Figure 30). The properties adopted for the shotcrete reinforcement layer with a reinforcement rate of 0.5% are in Table 6 and the compressive strength of the steel was considered null, due to the mesh is composed of thin bars and unlikely to contribute to the compressed regions. The reinforced vault maintains a predominantly linear behavior up to a load factor 3.0 times its own weight, about 60% higher than the original model, with a factor of 1.9. From that point on, the strengthened structure loses linearity, converging to the original condition. It can be thus stated that the applied strengthening measures provided increasing capacity against cracking but, in terms of ultimate condition, the gain is marginal.
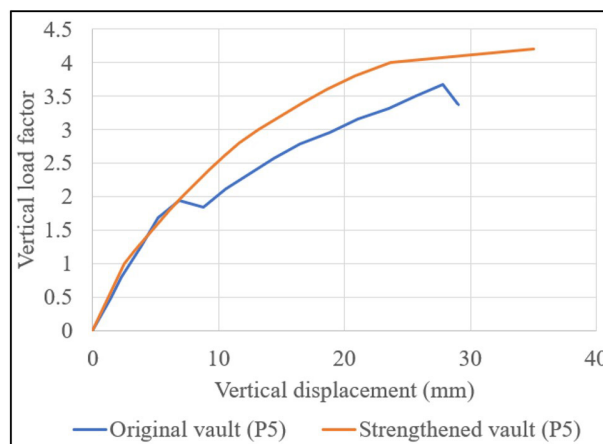


**Figure 30** – Gravitational load capacity of vault in the original and strengthening condition.

## 4.6. Final remarks

The numerical analyses allowed the understanding of the behavior of the structure and its masonry domes and vault, concluding that: (a) the vault's performance is highly affected by the vulnerability of the supports to differential settlements; (b) the vault is the structural component more likely to suffer damage and collapse in case of increasing gravitational loading; (c) the potential collapse mechanism of the vault under the effect of gravitational loading is associated with the rotation of the support in the main facade, which has no lateral bracing; (d) the domes proved to be very stiff and very resistant to gravitational loading; (e) the domes were affected by the distortion caused by differential settlements in their supports; (f) compared to the real damage manifested, the analyses indicate a 25% to 50% reduction in soil stiffness at the base of both internal walls and the pillar of Av. Treze de Maio, during underground excavation works; (g) the intervention carried out in the 1970s provided higher cracking resistance to the vault under gravitational loading, demonstrating the long-term resilience of the material, with no signs of damage since then.

## 5 CONCLUSIONS

The article demonstrates the importance of a historical, experimental and numerical multidisciplinary approach for the structural analysis and evaluation of the integrity of historic monuments, using the masonry domes and vault of the Theatro Municipal of Rio de Janeiro, as a case study.

Throughout the documental research, it was found that the construction sequence can be considered as a demonstration of the technological advances of the early 20th century, with emphasis on the mixed structural system, design measures for firefighting and construction management tools; the structural interventions that occurred in the past used advanced techniques and materials, for the period in which they were made; the information in the documents accessed were essential for the interpretation and measurement of the tests made in situ.

The experimental program provided data that confirmed and complemented the information from the archival research, such as geometric data, constructive data and mechanical properties data that could be compared by different tests, without causing damage to the structural and decorative elements. This information was useful for the elaboration and validation of the numerical model. The experimental data can be used as reference for preventive and periodic monitoring of the integrity of the domes and vault and the integrated paints, as well as to control possible future interventions.

The numerical analyses considered the non-linear behavior of the materials, the constructive phases, and the soil-structure interaction, once the numerical model was generated, calibrated, and considered valid to represent the current behavior of the studied structure. Different configurations of soil stiffness were analyzed and made it possible to assess the situation of differential settlement that best reproduced the damage pattern mapped from reports from the 1970s and thermographic images. Nonlinear static analyzes were performed to estimate the ability of the domes and vault to sustain gradually increasing gravitational loads and eventual collapse modes in the original and subsequent reinforcement situations. In addition, the results show that the corrective measures taken in the 1970s have ensured a longer lifespan to the vault and domes, restoring the load capacity of the structure and demonstrating the resilience of the material in the long term, as no signs of damage are currently found.

Although the adopted methodology has proved to be useful to evaluate the structural behavior of the masonry domes and vaults and validate some of the proposed considerations, it is recommended that additional work be carried out in order to improve the presented results, such as the continuity of the experimental program using equipment more sensitive and with more advanced technology, in order to apply different physical principles related to the investigated properties. It is suggested the flat jack test to confirm the mechanical properties in the brick masonry samples already prepared, the application of GPR with a higher frequency antenna for greater accuracy in the thickness of the domes and vault, in addition to the improvement in the geometric and numerical modeling.

## ACKNOWLEDGEMENTS

## REFERENCES

[1]   A. Tralli, C. Alessandri, and G. Milani, "Computational methods for masonry vaults: A review of recent results," *Open Civ. Eng. J.*, vol. 8, pp. 272–287, 2014, http://dx.doi.org/10.2174/1874149501408010272.

[2]   S. Huerta Fernández, "Diseño estrutural de arcos, bóvedas y cúpulas na España – ca. 1500 ~ ca. 1800," Ph.D. dissertation, Univ. Politéc. Madrid, Madrid, 1990.

[3]   S. Huerta Fernández, *Arcos, Bóvedas y Cúpulas – Geometria y Equilibrio en el Cálculo Tradicional de Estructuras de Fábrica.* Madrid: Inst. Juan de Herrera, 2004.

[4]   S. Acikgoz, K. Soga, and J. Woodhams, "Evaluation of the response of a vaulted masonry structure to differential settlements using point cloud data and limit analyses," *Constr. Build. Mater.*, vol. 150, pp. 916–931, 2017.

[5]   M. D. Boscardin and E. J. Cording, "Building response to excavation-induced settlement," *J. Geotech. Eng.*, vol. 115, pp. 1–21, 1989.

[6]   J. B. Burland and C. P. Wroth, "Settlement of building and associated damage," in *Proc Br. Geotech. Soc. Conf. Settl. Struct.*, London, 1974, pp. 611–654.

[7]   J. F. T. Jucá, "Influência de escavações nos recalques em edificações vizinhas," M.S. thesis, Fed. Univ. Rio de Janeiro, Rio de Janeiro, 1981.

[8]   Ellowitz J., "Structure and history of Guastavino vaulting at the Metropolitan Museum of Art," M.S. thesis, Massachusetts Inst. Technol., Massachusetts, 2014.

[9]   G. Cardani and L. Binda, "Guidelines for the masonry quality evaluation in built heritage," *Built Herit. Monit. Conserv. Manage.*, vol. 2013, pp. 107–115, 2013.

[10]  B. Tejedor, E. Lucchi, D. Bienvenido-Huertas, and I. Nardi, "Non-destructive techniques (NDT) for the diagnosis of heritage buildings: traditional procedures and futures perspectives," *Energy Build.*, vol. 263, pp. 112029, 2022., http://dx.doi.org/10.1016/j.enbuild.2022.112029.

[11]  International Council of Monuments and Sites, *Recommendations for the Analysis, Conservation and Structural Restoration of Architectural Heritage*. Paris: ICOMOS, 2001.

[12]  L. Barazzetti, L. Binda, M. Scaioni, and P. Taranto, "Photogrammetric survey of complex geometries with low-cost software: application to the 'G1′ temple in Myson, Vietnam," *J. Cult. Herit.*, vol. 12, pp. 253–262, 2011, http://dx.doi.org/10.1016/j.culher.2010.12.004.

[13]  B. Bayram, G. Nemli, T. Özkan, O. E. Oflaz, B. Kankotan, and İ. Çetin, "Comparison of laser scanning and photogrammetry and their use for digital recording of cultural monument case study: Byzantine Land Walls-Istanbul," in *ISPRS Ann. Photogramm. Remote Sens. Spat. Inf. Sci.*, Taipei, Taiwan, 2015, pp. 17–24. https://doi.org/0.5194/isprsannals-II-5-W3-17-2015.

[14]  B. Riveiro, J. C. Caamaño, P. Arias, and E. Sanz, "Photogrammetric 3D modelling and mechanical analysis of masonry arches: an approach based on a discontinuous model of voussoirs," *Autom. Construct.*, vol. 20, pp. 380–388, 2011, http://dx.doi.org/10.1016/j.autcon.2010.11.008.

[15]  L. J. Sánchez-Aparicio, B. Riveiro, D. González-Aguilera, and L. F. Ramos, "The combination of geomatic approaches and operational modal analysis to improve calibration of finite element models: a case of study in Saint Torcato Church (Guimarães, Portugal)," *Constr. Build. Mater.*, vol. 70, pp. 118–129, 2014, http://dx.doi.org/10.1016/j.conbuildmat.2014.07.106.

[16]  T. Luhmann, S. Robson, S. Kyle, and I. Harley, *Close Range Photogrammetry - Principles, Techniques and Applications*. Dunbeath: Whittles Publ., 2006. https://doi.org/10.1111/phor.12114.

[17]  C. Meola, G. M. Carlomagno, and L. Giorleo, "The use of infrared thermography for materials characterization," *J. Mater. Process. Technol.*, vol. 155–156, pp. 1132–1137, 2004, http://dx.doi.org/10.1016/j.jmatprotec.2004.04.268.

[18]  C. Meola, "Infrared thermography in the architectural field," *ScientificWorldJournal*, vol. 2013, pp. 1–8, 2013, http://dx.doi.org/10.1155/2013/323948.

[19]  B. Milovanović and I. Banjad Pečur, "Review of active IR thermography for detection and characterization of defects in reinforced concrete," *J. Imaging*, vol. 2, no. 2, pp. 11, 2016, http://dx.doi.org/10.3390/jimaging2020011.

[20]  A. Kylili, P. A. Fokaides, P. Christou, and S. A. Kalogirou, "Infrared thermography (IRT) applications for building diagnostics: a review," *Appl. Energy*, vol. 134, pp. 531–549, 2014, http://dx.doi.org/10.1016/j.apenergy.2014.08.005.

[21]  C. Maierhofer, M. Röllig, and J. Schlichting, "Active thermography for evaluation of reinforced concrete structures," in *Non-Destructive Evaluation of Reinforced Concrete Structures: Non-Destructive Testing Methods, vol. 2*. Cambridge, UK: Woodhead Publ., 2010, p. 370–402.

[22]  H. D. Young and R. A. Freedman, *Física II – Termodinâmica e Ondas*, 12a ed. São Paulo: Addison Wesley, 2008.

[23]  L. F. B. Miranda, "Ensaios acústicos e de macacos planos em alvenarias resistentes," Ph.D. dissertation, Fac. Eng., Univ. Porto, Porto, 2011.

[24]  L. Qixian and J. H. Bungey, "Using compression wave ultrasonic transducers to measure the velocity of surface waves and hence determine dynamic modulus of elasticity for concrete," *Constr. Build. Mater.*, vol. 10, no. 4, pp. 237–242, 1996, http://dx.doi.org/10.1016/0950-0618(96)00003-7.

[25]  B. J. Lee, S.-H. Kee, T. Oh, and Y.-Y. Kim, "Evaluating the dynamic elastic modulus of concrete using shear-wave velocity measurements," *Adv. Mater. Sci. Eng.*, vol. 2017, pp. 1, 2017, http://dx.doi.org/10.1155/2017/1651753.

[26]  T. Naik, V. M. Malhotra, and J. S. Popovics, "The ultrasonic pulse velocity method", in *Handbook on Nondestructive Testing of Concrete*, 2nd ed., V. M. Malhotra and N. J. Carino, Eds., CRC Press; 2003, pp. 8–19.

[27]  D. J. Daniels, *Ground Penetrating Radar*, 2nd ed. London: Inst. Electr. Eng., 2004.

[28]  K. Dinh, N. Gucunski, and T. Zayed, "Automated visualization of concrete bridge deck condition from GPR data," *NDT Int.*, vol. 102, pp. 120–128, 2019.

[29]  A. B. F. Benedetto, "Application field – specific synthesizing of sensing technology – civil engineering application of ground penetrating radar sensing technology," *Ref Modul Mater Sci Mater Eng Compr Mater Process*, vol. 13, pp. 393–425, 2014.

[30]  A. P. Annan, *Ground Penetrating Radar – Principles, Procedures & Applications*. Mississauga, Canada: Sensors and Software Inc., 2003.

[31]  W. W. L. Lai, X. Dérobert, and A. P. Annan, "A review of Ground Penetrating Radar application in civil engineering: A 30-year journey from Locating and Testing to Imaging and Diagnosis," *NDT Int.*, vol. 96, pp. 58–78, 2018.

[32]  F. M. C. P. Fernandes, "Evaluation of two novel NDT techniques – microdrilling of clay bricks and ground penetrating radar in masonry," Ph.D. dissertation, Univ. Minho, Guimarães, 2006.

[33] G. Tronca, S. Lehner, L. Raj, I. Tsalicoglou, J. Meier, and R. Mennicke, "Looking into concrete – multiple frequency usage in radar products to detect structural parameters and defects faster and more accurately," in *Proc. 15th Asia Pacific Conf. Non-Destructive Test*, Singapore, 2017.

[34] J. H. Bundey, S. G. Millard, and M. G. Grantham, *Testing of Concrete in Structures*, 4th ed. London: Taylor & Francis, 2006.

[35] S. A. Proceq, *Profometer – Operating Instructions*. Switzerland: Proceq SA, 2017.

[36] A. Cunha, E. Caetano, F. Magalhães, and C. Moutinho, "Recent perspectives in dynamic testing and monitoring of bridges," *Struct. Contr. Health Monit.*, vol. 20, pp. 853–877, 2012.

[37] B. M. Douglas and W. H. Reid, "Dynamic tests and system identification of bridges," *J. Struct. Div.*, vol. 108, pp. 2295–2312, 1982.

[38] N. Mendes, "Seismic assessment of ancient masonry buildings: shaking table tests and numerical analysis," Ph.D. dissertation, Univ. Minho, Guimarães, 2012.

[39] G. Karanikoloudis, P. B. Lourenço and N. Mendes, Structural monitoring of induced vibrations from underground railway traffic in the Carmo Convent, in Lisbon. 2017.

[40] I. Lombillo, L. Villegas, E. Fodde, and C. Thomas, "In situ mechanical investigation of rammed earth: Calibration of minor destructive testing," *Constr. Build. Mater.*, vol. 51, pp. 451–460, 2014.

[41] E. Cescatti, M. D. Benetta, and C. Modena, "Analysis and evaluations of flat jack test on a wide existing masonry buildings sample", in *Brick Block Mason – Trends, Innovations and Challenges*, C. Modena, F. Porto and M. R. Valluzzi, Eds., London: CRC Press, 2016, pp. 1485–1491.

[42] M. D. O. Soriani, E. R. Sanches, and G. A. Parsekian, "An overview of the use of flatjacks for nondestructive testing," in *Proc. 12th North Am. Mason. Conf.*, Denver, Colorado: The Masonry Soc., 2015.

[43] A. Borri, M. Corradi, G. Castori, and A. De Maria, "A method for the analysis and classification of historic masonry," *Bull. Earthquake Eng.*, vol. 13, no. 9, pp. 2647–2665, 2015, http://dx.doi.org/10.1007/s10518-015-9731-4.

[44] A. Borri, M. Corradi, A. De Maria, and R. Sisti, "Calibration of a visual method for the analysis of the mechanical properties of historic masonry," *Procedia Struct. Integr.*, vol. 11, pp. 418–427, 2018, http://dx.doi.org/10.1016/j.prostr.2018.11.054.

[45] A. Borri, M. Corradi, and A. De Maria, "The failure of masonry walls by disaggregation and the Masonry Quality Index," *Heritage*, vol. 3, no. 4, pp. 1162–1198, 2020, http://dx.doi.org/10.3390/heritage3040065.

[46] E. P. Machado, "A cobertura do Theatro Municipal do Rio de Janeiro: restauração ou reconstrução?," M.S. thesis, Iphan, Rio de Janeiro, 2012.

[47] Instituto do Patrimônio Histórico e Artístico Nacional, *Lista dos Bens Tombados e Processos em Andamento (1938-2018)*. Rio de Janeiro: Iphan, 2018. http://portal.iphan.gov.br/uploads/ckfinder/arquivos/Lista_bens_tombados_processos_andamento_2018 (accessed Dec. 10, 2018).

[48] F. O. Passos, *Projeto Áquila - Theatro Municipal do Rio de Janeiro*. Rio de Janeiro, 1904.

[49] Comissão Construtora do Theatro Municipal, "Relatório histórico – 1909" in *Theatro Municipal do Rio Janeiro – Edição Comemorativa 100 anos*, C. Ferrão and J. P. M. Soares, Ed., Rio de Janeiro: Kapa Ed., 2009, pp. 278–282.

[50] Kennedy, *Álbum Comemorativo da Remodelação do Theatro Municipal.* 1934.

[51] Shewing Steel Work & Frazzi, *Theatro Municipal - Plan of Roof - Drawing nº 8*. 1905.

[52] P. Moreira, *Photo TMRJ.* 1975. https://acervo.oglobo.globo.com (accessed Dec. 7, 2022).

[53] Sondotécnica, *Exame das Fundações do Theatro Municipal do Rio de Janeiro, Relatório EG-620/69*. Rio de Janeiro, 1969.

[54] FUNTERJ, *Vistoria do Prédio do Theatro Municipal do Rio de Janeiro – Considerações Gerais*. Rio de Janeiro, 1975.

[55] L. M. Schiros, "Recuperação estrutural das cúpulas do foyer do Theatro Municipal do Rio de Janeiro," in *Colóq. Patol. Concr. Recuper. Estrut.*, 1978, pp. 188–204.

[56] L. A. Camara, *Parecer Técnico de Engenharia – Avaliação das Causas do Desabamento do Ed. Liberdade.* Rio de Janeiro, 2012.

[57] A. C. J. Evangelista, "Avaliação da resistência do concreto usando diferentes ensaios não destrutivos," Ph.D. dissertation, COPPE, Univ. Fed. Rio de Janeiro, Rio de Janeiro, 2002.

[58] L. Binda and A. Saisi, "Non Destructive Testing applied to historic buildings: the case of some Sicilian Churches," in *Proc. 3rd Int. Semin. Hist. Constr. Possibilities Numer. Exp. Tech.*, Guimarães, Portugal, 2001, pp. 29–46.

[59] D. C. B. Cintra, "Ensaios não destrutivos em estruturas," in *Concreto Estrutural – Análise, Dimensionamento e Patologias*, E. S. Sánches Fo., Ed., Rio de Janeiro: Interciência, 2023, pp. 389–429.

[60] D. C. B. Cintra, E. S. Sánchez Fo., and D. M. Roehl, "Caracterização das cascas em alvenaria do Theatro Municipal do Rio de Janeiro," *Rev Port Eng Estrut.*, no. 10, pp. 39–50, 2019.

[61] X. Yang, P. Grussenmeyer, M. Koehl, H. Macher, A. Murtiyoso, and T. Landes, "Review of built heritage modelling: Integration of HBIM and other information techniques," *J. Cult. Herit.*, vol. 46, pp. 350–360, 2020, http://dx.doi.org/10.1016/j.culher.2020.05.008.

[62] Y. El Masri and T. Rakha, "A scoping review of Non-Destructive Testing (NDT) techniques in building performance diagnostic inspections," *Constr. Build. Mater.*, vol. 265, pp. 120542, 2020, http://dx.doi.org/10.1016/j.conbuildmat.2020.120542.

[63] Associação Brasileira de Normas Técnicas, *Concreto Endurecido – Avaliação da Dureza Superficial Pelo Esclerômetro de Reflexão – Método de Ensaio*, ABNT NBR 7584, 2012.

[64] Proceq SA, *Silver Schmidt – Instruções de Operação*. Switzerland: Proceq SA, 2016.

[65] Associação Brasileira de Normas Técnicas, *Determinação da Velocidade de Propagação de Onda Ultrassônica*, ABNT NBR 8802, 2019, 11 p.

[66] D. C. B. Cintra, P. M. B. Manhães, F. M. C. P. Fernandes, D. M. Roehl, J. T. Araruna Jr, and E. S. Sánchez Fo, "Evaluation of the GPR (1.2 GHz) technique in the characterization of masonry shells of the Theatro Municipal do Rio de Janeiro," *Ibracon Struct Mater J*, vol. 13, pp. 274–297, 2020.

[67] E. R. Sanches, *Avaliação Não Destrutiva Com Técnica de Macacos Planos e a Fazenda do Pinhal*. São Carlos: Univ. Fed. São Carlos, 2017.

[68] American Society for Testing and Materials, *Standard Test Method for in Situ Measurement of Masonry Deformability Properties Using the Flatjack Method*, ASTM C1197-14, 2014. https://doi.org/10.1520/C1197-14A.

[69] Italia. Ministero delle Infraestrutture e dei Trasporti, "Norme Tecniche per le Costruzioni" approvate con decreto ministeriale 17 gennaio 2018," *Gazz. Uff.*, 2018.

[70] R. R. Álvarez de Lara, "Structural analysis of the church of the Monastery of São Miguel de Refojos," M.S. thesis, Univ. Minho, Guimarães, 2016.

[71] G. Karanikoloudis, "Canterbury Cathedral - structural analysis of the south aisle," M.S. thesis, Univ. Minho, Guimarães, 2014.

[72] L. Rovero and F. Fratini, "The Medina of Chefchaouen (Morocco): a survey onmorphological andmechanical features of the masonries," *Constr. Build. Mater.*, vol. 47, pp. 465–479, 2013.

[73] Structural Vibrations Solutions, *ARTeMIS Modal 5.3.1.1 - x64*. 2018.

[74] R. Brincker, L. Zhang, and P. Andersen, "Modal identification of output-only systems using frequency domain decomposition," *Smart Mater. Struct.*, vol. 10, pp. 441–445, 2001.

[75] M. P. Rios, "Structural performance of shells of historical constructions – the Municipal Theatre of Rio de Janeiro," M.S. thesis, Univ. Minho, Guimarães, 2017.

[76] DIANA FEA BV, *DIANA Finite Element Analysis - Release 10.2.* 2017.

[77] J. S. P. Panitz, "Desenvolvimento e implementação de metodologias para a determinação da deformabilidade e tensões em maciços gnássicos," M.S. thesis, Pontif. Univ. Catol. Rio de Janeiro, Rio de Janeiro, 2008.

[78] A. D. Figueiredo, "Concreto projetado – fatores intervenientes no controle da qualidade do processo," M.S. thesis, Univ. São Paulo, 1992.

[79] W. Bates, *Historical Structural Steelwork Handbook*. London: The Chameleon Press, 1984.

[80] A. H. Teixeira and N. S. D. Godoy, "Análise, projeto e execução de fundações rasas," in *Fundações - Teoria e Prática*, 2nd ed., W. Hachich, F. F. Falconi, J. L. Saes, R. G. O. Frota, C. S. Carvalho and S. Niyama, Eds., São Paulo: Pini; 1998, pp. 227–264.

[81] F. Brandão, E. Mesquita, A. Diógenes, P. Antunes, and H. Varum, "Caracterização dinâmica de uma edificação histórica do século XIX," *Rev. IBRACON Estrut. Mater.*, vol. 11, pp. 52–75, 2018.

[82] DIANA FEA BV, *User's Manual Release 10.2.* 2017.

[83] G. Gazetas, J. L. Tassoulas, R. Dobry, and M. J. O'Rourke, "Elastic settlement of arbitrarily shaped foundations embedded in half-space," *Geotechnique*, vol. 35, pp. 339–346, 1985, http://dx.doi.org/10.1680/geot.1985.35.3.339.